The Abundances of Methane and *Ortho/Para* Hydrogen in Uranus and Neptune: Implications of New Laboratory 4-O H_2 Quadrupole Line Parameters

Kevin 11. Baines

Jet I'repulsion laboratory
California Institute of Technology
4800 Oak Grove Drive
Pasadena, California 91109
(818) 354-0481
kbaines@aloha.jpl.nasa.gov

Michael E. Mickelson and Lee. E. Larson

Denisen [University
Granby, Ohio

and

David W. Ferguson

Ohio State University
Columbus, Ohio

Submitted to Icarus, July 8, 1994

Manuscript Pages: 37
Number of Figures: 13

Key Words: Uranus, Atmosphere
Neptune, Atmosphere
Abundances, Atmospheres
Atmospheres, Composition
Atmospheres, Structure

Proposed Running Head:

CH_4 and 112 in Uranus and Neptune

Send Editorial Correspondence and Proofs to:

Dr. Kevin H. Baines

M/S 169-237

Jet Propulsion laboratory

4800 Oak Grove Drive

Pasadena, Ca. 91109

81S-354-0481

E-Mail: kbaines@aloha.jpl.nasa.gov

FAX: 818-393-4619

ABSTRACT

The tropospheric methane molar fraction ($f_{CH4,t}$) and the *ortho/para* hydrogen ratio are derived for Uranus and Neptune based on new determinations of spectroscopic parameters for key hydrogen features as reported by Ferguson et *al.* (1 993, *J. Mol. Spec 160,* 315 - 325). For each planet, the relatively weak laboratory linestrengths (approximately 30% and 15% less than the theoretical 4-O S(0) and S(1) linestrengths, respectively) results, when compared to analyses adopting theoretical values, in a *-30%* decrease in the tropospheric methane ratio and a comparable increase in the pressure level of the optically-thick cloudtop marking the bottom of the visible atmosphere (P_{cld}). The increase in the ratio of S(1)/s(0) linestrengths from 4.4 (theoretical) to - 5.9 (measured) results in a decrease in the range of viable *ortho/para* ratios; an equilibrium hydrogen distribution is now the best fit for both planets. For Uranus, we find $f_{CH4,t} = 0.016_{-0.005}^{+0.007}$, $P_{cld} = 3.2_{-.3}^{+1.00}$ bars, and $0.85 < f_{eH2} < 1.00$ (where f_{eH2} and $1-f_{eH2}$ denote the fraction of H_2 in the equilibrium and normal state, respectively) compared to the Baines and Bergstralh (1986, *Icarus* 56, 543-559) values of $f_{CH4,t} = 0.030_{-0.010}^{+0.016}$ $P_{cld} = 2.7_{-0.4}^{+0.5}$ bars, and $0.63 < f_{eH2} < 0.95$. For Neptune, we find $f_{CH4,t} = 0.022_{-0.006}^{+0.005}$, $P_{cld} = 3.8_{-0.3}^{+0.7}$ bars, and $0.89 < f_{eH2} < 1.0$ compared to the Baines and Smith (1990, *Icarus* 85, 65-108) values of $f_{CH4,t} = 0.03 \pm 0.007$, $P_{cld} = 3.3_{-0.1}^{+0.5}$ bars, and $0.85 < f_{eH2} < 1.0$. The methane mixing ratio reported here are in agreement with the value of 0.023

derived by the Voyager Radio Occulatation Experiment (Lindal 1992, *Astron. J.* 103, 967 - 982) for Neptune, but slightly lower than the. Voyager Uranus measurement of 0023 reported by Lindal *et al.* (1987, *JGR* 92, 14987 - 15001). The relative carbon-to-hydrogen abundances of $20\ ^{+9}_{-6}$ and $28\ ^{+7}_{-8}$ times the solar value of $4.7\ 10^{-4}$ derived by Lambert (1 978, *Mon. Not. Roy. Astron. Sot.* **192**, *249-272)* for Uranus and Neptune supports planetary formation mechanisms involving the dissolution of carbon-bearing planetesimals in the atmospheres of both planets during their early stages of formation (e. g., Pollack *et al.*, 1986, *Icarus* 67, 409-443).

1, INTRODUCTION

The deep-atmosphere methane mixing ratio and *ortho-para* hydrogen abundances in Uranus and Neptune, key factors in assessing current theories of planetary formation and evolution (Pollack *et al.*, *1986,* Bodenheimer and Pollack, 1986) and planetary circulation and vertical dynamics (e. g., Conrath and Gierasch, 1984), have proven difficult to measure in the outermost Jovian planets For example, the Voyager IRIS experiment, which successfully measured the tropospheric methane abundance, $f_{CH4,t}$, in Jupiter (Gautier *et* al., 1982) and Saturn (Courtin *et al.*, 1984) was unable to measure $f_{CH4,t}$ in Uranus and Neptune, principally due to the exceedingly cold temperatures extant in these remote atmospheres, For Uranus, the low thermal flux produced at such low temperatures

(about 100 K just below the tropospheric methane cloud) renders difficult observations of the CH_4 emission spectrum at its fundamentals near 3.3 and 7.8-μm. For Neptune, the relatively hot and methane-rich stratosphere readily emits radiation in these bands which then obscures emission emanating from deeper regions of the atmosphere. The lack of signal has proved direct tropospheric methane detection difficult as well using earth-based thermal radiance measurements. In the tropospheric-sensitive millimeter/submillimeter regime, Orton *et al. (1* 986) derived CH4 mixing ratios for Uranus and Neptune from matching the observed temperature structure to that predicted for various ωet adiabatic lapse rates associated with different methane mixingratios. However, the poor S/N data together with uncertain gas and particulate extinction effects resulted in loose constraints on $f_{CH4,t}$: Nominal values near *0.02* were found for both planets, with the large uncertainties encompassing values from approximately 0.005 to 0.03. As for the *ortho/para* distribution of hydrogen, Orton *et al* (1986) found that an equilibrium hydrogen distribution was consistent with their data, assuming that the hydrogen-dominated lapse rate was that predicted by 112 in "frozen" equilibrium wherein the specific heat at each level in the atmosphere is calculated as the weighted sum of the individual specific heats of *ortho*-H_2 and *para*-H_2. which are presumed populated in equilibrium at the ambient temperature (Cf.., Trafton 1967). However, this technique does not allow direct determination of the *ortho/para* distribution.

Consequently, unlike Jupiter and Saturn, the determination of the tropospheric methane mixing ratio and *ortho/para* distribution of hydrogen in Uranus and Neptune has relied largely on ground-based observations in the visible, most notably on spectral observations of individual, isolated CH_4 and H_2 lines (e.g., Baines 1983; Baines and Bergstralh, 1986; Baines and Smith, 1990). However, largely due to the increased effect of aerosols at these wavelengths, the determination of molecular abundances - in particular, tropospheric mixing ratios - is less straightforward than at longer wavelengths. The troposphere of the major planets are characterized by condensation clouds and hazes which - particularly in the visible - obscure observations of absorption features formed below them. On Jupiter and Saturn, NH_3 and lower lying clouds obscure the interpretation of NH_3 mixing ratios (e. g., Baines *et al.*,]989); on Uranus and Neptune, CH_4 hazes and an optically thick lower layer obscure the interpretatation of the deep-atmosphere methane abundance.

previous investigations (*e.g.*, Baines and Bergstralh, 1986; Baines and Smith, 1990) utilized a combined analysis of well-isolated hydrogen quadruple and methane lines to simultaneously determine the tropospheric methane mixing ratio and the cloudtop pressure level of the optically thick aerosol layer marking the bottom of the visible atmosphere for each of the outermost giant planets, Uranus and Neptune, By utilizing observations of hydrogen absorption produced in both odd and even rotational quantum states, these investigators were also able to determine the

tropospheric *ortho/para* hydrogen distribution, important for understanding timescales of vertical convection and circulation from the relatively deep interior (e. g., Conrath and Gierasch,1984; Smith 1978).

however, these previous investigations were hampered somewhat by imperfect knowledge of hydrogen quadruple absorption characteristics, most notably the pressure shift coefficients and room-temperature linestrengths of the H_2 4-o s(o) and S(1) lines. In particular, the pressure shift for the 4-O S(0) line has not, prior to Ferguson *et al.* (1993), been measured in the laboratory, The S(1) line pressure shift, measured once in the laboratory. by Brault and Smith (1980), indicated a shift some 20% less than the theoretical value derived by McKellar (1974). Nevertheless, these researchers and others (*e.g.*, Cochran and Smith,1983) consistently resorted to the theoretically derived values. Similarly, line strengths have been measured in the laboratory (e. g., Bragg *et* al., 1982; Brault and Smith, 1980; Trauger *et al.*, 1978; Bergstralh *et al.*, 1978), but they have consistently fallen short of the theoretical strengths (e. g., Poll and Wolniewicz, 1978). Nevertheless, the previous analyses of Uranus and Neptune have again all resorted to the theoretical values, based on the marginal agreement between the then-current measurements of Brault and Smith (1980) and Bragg *et al.* (1 982) for the stronger S(1) line. However, the most recent improved linestrength measurements of Ferguson *et al.* (1993) indicate that these lines are indeed substantially weaker than their theoretical values, - by 15% in the

case of S(1) and 30% in the case of S(0). Moreover, the pressure shift coefficients were determined by these researchers to be 30-60% less than the theoretical values. Both of these effects serve to weaken the ability of hydrogen to absorb light, thus indicating that substantially more hydrogen is present in the observable atmosphere than reported by recent investigations. in this paper, we re-evaluate the tropospheric aerosol structure and molecular abundances of methane and *ortho/para* hydrogen based on these new laboratory findings, essentially updating the previously reported tropospheric atmospheric parameters reported by Baines and Bergtralh (1986) and Baines and Smith (1 990).

11. THE OBSIH{VATIONS

nigh-spectra] resolution observations of the 4-O S(0) and S(1) hydrogen quadrupole lines and the 6818.9-Å CH_4 feature are utilized to constrain (1) the methane mixing ratio of the deep atmosphere below the methane condensation level, (2) the cloudtop pressure level of the aerosol layer marking the bottom of the visible atmosphere, and (3) the mean ratio of *ortho*-to-*para* hydrogen. As previously demonstrated by Baines and Bergstralh (1 986) for Uranus and by Baines and Smith (1 990) for Neptune, the observed ratio of H_2 equivalent widths constrains the *ortho/para* distribution, while the individual equivalent widths constrain the relationship between the methane haze opacity ant] the cloudtop pressure of the optically-

thick cloud deck. Alternatively, when the methane haze opacity is known, these lines constrain this cloudtop pressure, P_{cld}, and the tropospheric methane mixing ratio, $f_{CH4,t}$. As in the previous work, here we use the latter procedure given that broadband constraints, notably from Baines and Bergstralh (1986) for Uranus and Baines and Hammel (1994) for Neptune, place significant limits on the methane haze opacity. These lines, which due to not-insignificant pressure shifts and pressure broadening are unsaturated, increase in equivalent width as P_{cld} increases, but decrease as $f_{CH4,t}$ increases.

The 6818.9-Å methane line observed by Baines *et al.* (1983) on both Uranus and Neptune can be used as well to jointly constrain $f_{CH4,t}$ and P_{cld}. Contrary to the behavior of the hydrogen lines, the equivalent width of the methane line increases as $f_{CH4,t}$ increases. Thus, as demonstrated by Dairies and Bergstralh (1986) and Baines and Smith (1990), the combined analysis of H_2 and CH_4 line equivalent widths sets relatively tight limits on both $f_{CH4,t}$ and P_{cld}.

For hydrogen in Uranus, we analyze the high-spectral resolution observations of Trauger and Bergstralh (1981) previously analyzed by Baines and Bergstralh (1986). Equivalent widths of 24.2 ± 0.5 mÅ and 25.3 ± 0.5 mÅ are reported for the 1124-O S(1) and S(0) lines, respectively. For Neptune, we utilize the observations of Smith *et al.* (1989), previously analyzed by Baines and Smith (1990), for which equivalent widths of 19.2 ± 2.4 mÅ and 23.7 ± 2.4 mÅ are reported respectively for the S(1) and S(0) features. The methane line

measurements by Baines *et al.* (1 983) are characterized by a spectral resolution of 100 mÅ and a signal-to-noise ratio of better than 40-to-1. The line exhibits an equivalent width of 130 ± 10 mÅ for Uranus, 150 ± 10 mÅ for Neptune.

111. PARAMETERIZATION/PROCEDURE

The analysis procedure follows largely that of Baines and Bergstralh (1986) for Uranus and Baines and Smith (1990) for Neptune, utilizing the updated radiative transfer code of Baines and Hammel (1 994). The previous work on tropospheric methane and *ortho/para* hydrogen is revised to include: (1) the use of Voyager-determined parameters, including thermal profiles, helium abundances, and aerosol phase functions, (2) the use of low-temperature methane absorption coefficients (Karkoschka and Tomasko, 1992), and (3), in the case of Neptune, vertically-increasing methane molar fractions in the warm stratosphere.

111. A Molecular Spectral Properties

For hydrogen, we use the Galatry (1961) line shape to calculate the wavelength-dependent H_2 extinction produced within each atmospheric layer, incorporating the recent line strength, pressure broadening, and pressure shift measurements of Ferguson *et al.*

(1993). While comparable to earlier measurements of Bragg *et al.* (1982) and Brault and Smith (1 980), and substantially larger than the prior measurements of Trauger et *al.* (1 978) and Bergstralh *et al.* (1978), the measured line strengths are nevertheless significantly less than the theoretical line strengths of Poll and Wolniewicz (1978) adopted in earlier analyses of the troposphere of Uranus and Neptune (e. g., Baines and Bergstralh, 1986; Baines and Smith, 1990; Smith and Baines, 1990). In particular, for the 4-O S(1) feature, we use the range of linestrengths $1.37 \pm 0.17\ 10^{-4}$ cm^{-1}/(km-am) in our analysis, as opposed to the Poll and Wolniewicz theoretical value of $1.66\ 10^{-4}$ c m^{-1}/(km-am), while for the 4-O S(0) line we use 2.31 $\pm$ 0.55 10-5 as opposed to the theoretical value of $3.76\ 10^{-5}$. We use the full range of Ferguson *et al.* (1993) pressure broadening coefficients for each line: $-\ 9.13 \pm 1.39\ 10^{-3}$ and $7.10 \pm 1.97\ 10^{-3}$ c m^{-1}.atm at 296 K for the 4-O S(1) and S(0) lines, respectively. The nominal figures agree with the previously-measured values of Bragg (1 981). used in previous studies in this study, we evaluate model atmospheres over the 15-25% uncertainty determined by Ferguson et al. (1993). For pressure shifts, we adopt as well the full range of 4-O S(0) and S(1) room-temperature coefficients derived by Ferguson *et al.* (1993): $-4.22 + 0.36\ 10^{-3}$ and $6.29 \pm 1.29\ 10^{-3}$ cm^{-1} atm^{-1}. These values are some 30-60% less than the theoretically-derived value of $-9.36\ 10^{-3}$ reported by McKellar (1974).

For extrapolation to the cold temperatures (-90 K at 1 bar) of these planetary troposphere, we adopt McKellar's (1974) empirically-determined temperature dependence for the pressure-

shift. On the other hand, the temperature- dependence for pressure broadening is explicitly analyzed in this work through an analysis of the shapes of the highly-resolved 4-O S(0) and S(1) line profiles observed on Uranus when its high obliquity yielded a small Doppler broadening component due to planetary rotation. Two cases are explicitly explored: pressure-broadening temperature exponents of 0.32 and 0.75. The former value was adopted by Baines and Smith (1990), as inferred from the HD:H_2 broadening measurements of Keffer (1985). The latter value has been extensively utilized (*cf.*, McKellar, 1974; Baines and Bergstralh, 1986; Cochran and Smith, 1983) and is theoretically expected for quadrupole-quadrupole broadening (*c.f.* Townes and Schawlow, 1955; Birnbaum, 1967)

For the 681 8.9-A methane line, we utilize the room-temperature line strength previously reported by Baines (1983). The pressure broadening behavior of the hydrogen-broadened 681 8.9-Å methane line derived by Keffer *et al.* (1986) is used; i.e, $\gamma = 0.0883\ I' (T_o/T)^{0.53}$, where To = 295 K. For Uranus, broadening of line profiles by planetary rotation is, calculated utilizing a cloud-level planetary rotation period of 16.6 hr, *i. e.*, the mean period determined for features near 30 degrees S. latitude (Smith et al., 1986) representative of the area-mean latitude observed on the Uranian disk. For Neptune, a cloud-level planetary rotation period of 17.9 hr is adopted, as reported by Hammel and Buie (1 987) for a prominent cloud feature seen near 38 degrees South latitude.

111.11. Uranus Atmosphere

FIGURE 1

The adopted parametrization of the Uranus atmosphere is illustrated in Figure 1, consistent with a large body of theoretical and observational evidence pertaining to stratospheric and tropospheric aerosols, temperature profiles, and helium molar fractions. Hydrocarbon haze layers extend from the upper stratosphere to a tropospheric methane haze near 1.3 bars, as predicted theoretically from photochemical-thermodynamical models (e. g., Atreya and Romani, 1985) and observed by Voyager (Smith *et al.*, 1986; Pollack *et al.*, 1987). We adopt the number densities, particle modal radii, and condensation levels of primary upper-level haze constituents (diacetylene, C_4H_2; acetylene, ~2}12; and ethane, C_2H_6) specified by Pollack *et al. (1987).* These aerosols are treated as Mie scatterers using a log-norms] distribution of width σ = 1.35 for number densities. For each stratospheric hydrocarbon haze layer, the refractive index is chosen to be that of the dominant constituent in that layer (which is the species just below its respective condensation level). In the troposphere, the methane condensate hazetop is assumed situated at the level reported by the Voyager radio occultation experiment (Lindal *et al.*, 1987), while its bottom is assumed located at the methane condensation temperature (which varies with the cieep-tropospheric methane mixing ratio). A double Henyey-Greenstein particle phase function is assumed for this layer (g_1 = 0.75, g_2 = -0.18, f_1 = 0,56), based on analysis of Voyager imagery over phase angle by Rages *et al.*(1 991). Below this methane

haze layer, of optical thickness τ_H, lies a clear region limited at its bottom by an optically-thick cloudtop at pressure P_{cld}, which itself is characterized by the same phase function as the methane haze. The therms] profile is that of Lindal *et al.* (1987). Below the methane cloud, the methane mixing ratio is fixed at its deep-tropospheric value. Following the Clausius-Clapeyron relation, this mixing ratio decreases with altitude in the cold-trap region above the methane condensation level. Above the tropopause, the mixing ratio is fixed at its tropopause value of 10^{-6}

In our analysis, the values of six parameters are left free to be constrained by the data. Two involve molecular mixing ratios: $f_{CH4,t}$, the deep-tropospheric methane mixing ratio; and f_{eH2}, the fraction of *ortho/para* hydrogen distributed following the equilibrium distribution of states. The other four parameters involve aerosol characteristics: τ_H and ϖ_H, the opacity and single-scattering albedo of the methane haze; P_{cld}, the pressure of the top of the presumed optically-thick layer marking the bottom of the visible atmosphere; and ϖ_{cld}, the single-scattering albedo of this cloud. The data itself consists of (1) the 681 8.9-Å methane equivalent widths of Baines *et al.* (1 983), previously analyzed by Baines (1983) and Baines and Bergstralh (1 986), (2) the hydrogen quadruple 4-O S(0) and S(l) equivalent widths of Trauger and Bergs tralh (1981), previously analyzed as well by Baines and Bergstralh (1986), and the broadband (7-A resolution) geometric albedo observations at the molecular line positions (i. e., 6369 Å, 6435 Å, and 6818.9 Å) as measured by Neff *et al.* (1984, 1985). A range of methane absorption coefficients was

used for each broadband wavelength, ranging from those derived by Karkoschka *et al.* (1992) for a cold atmosphere to those measured by Giver (1 978) at room temperature.

III.C Neptune Atmosphere

FIGURE

The adopted structure of the Neptunian atmosphere is based largely on the structure derived for the global atmosphere by Baines and Hammel (1 994), which, as for Uranus, in turn is based on a large body of theoretical and observational evidence. As depicted in Figure 2, our morphology includes a stratospheric haze region principally comprised of ethane (C_2H_6) and acetylene (C_2H_2) aerosol layers, but with trace amounts of propane (C_3H_8), propylene (C_3H_6), diacetylene (C_4H_2), and HCN aerosols (Romani *et* al., 1993). The distribution of aerosols is that determined by Baines and Hammel (1994) for the mean globe, based on the condensation levels of Romani *et al.* (1989). in the troposphere, a methane haze of opacity at 0.6 μm of τ_H = 0.085 is adopted (Baines and Hammel, 1994), characterized by the double Henyey-Greenstein phase function parameters of Pryor *et al.* (1992): g_1 = 0.900, g_2 = -0.11, and f_1 = 0.42. The bottom cloud resides at a pressure to be determined by the analysis, and is characterized as well by the Pryor *et al.* (1 992) phase function. As for Uranus, the single-scattering albedo of this cloud is to be constrained as well by the analysis. The helium molar fraction is assumed to be 0.15 (Conrath *et al.*, 1991), and the pressure-temperature profile of Tyler *et al.* (1 989) is adopted.

IV. RESULTS

IV. A The Temperature Dependence of Pressure Broadening

Using the spectrally-resolved line profiles of Uranus, we first explored the temperature dependence of the hydrogen pressure-broadening coefficient. Specifically, we investigated the power-law exponent, α_{PB}, in the expression:

$$\gamma(T) = \gamma_0 P\ (\text{'l'}.\ /\text{'l'}\ )^{\alpha}\text{l'll, where}$$

γ is the pressure-broadening coefficient at temperature T, γ_0 is the coefficient at temperature T_0, and P is the pressure.. Over a wide range of atmospheric model structures, we found that the theoretical value of 0.75 pertaining to quadrupolar interactions (e. g., Birnbaum 1967) provides a much better fit than the empirical HD-HD value of 0.32 measured by Keffer (1985) and used in recent analyses (e. g., Baines and Smith, 1990; Smith and Baines, 1990).

FIGURE :

Figure 3 shows modelled vs observed line profiles for the nominal atmospheric structure derived in this work ($f_{CH4,t}$ = 0.16, f_{eH2} = 1.0, p_c]d = 3.13. bars, τ_{II} = 0.6,). Standard deviations become 50% less for the S(1) line, and 30% less for the S(0) line, when a. temperature index of 0.75 is used instead of 0.32. The trend of standard deviations over a range of pressures and room-temperature pressure-broadening coefficients is depicted in Figure 4. Superior fits

FIGURE 4

over the full range of pressures is for α_{PB} = 0.75 and the upper-limit values for γ_o measured by Ferguson *et al.* (1 993).

IV.B. Uranus

FIGURE 5

For each choice of $\tau_H, \varpi_H, f_{eH2}$, and $f_{CH4,t}$ (as described in Section III.B and depicted in Figure 1), the range of P_{cld} and ϖ_{cld} which fit the range of observed equivalent widths and continuum geometric al bedoes for each of the three molecular lines was determined. Evaluating over a range of $f_{CH4,t}$, a family of solutions in I'$_c$] d - $f_{CH4,t}$ space was developed for each molecular line, as, for example, depicted in Figure 5 for the case of τ_H =0.40, ϖ_H = 1.0, and f_{eH2} = 1.0. Each of the three molecular lines places relatively broad constraints on viable combinations of ($P_{cld}, f_{CH4,t}$). However, as depicted in Figure 6, the coupled constraints imposed by the three lines places tight constraints on viable (P_{cld} , $f_{CH4,t}$) combinations. in particular, uncertainties of ± 0.004 in $f_{CH4,t}$ and ± 0.5 bars in P_{cld} are found. Differences in the behaviors of hydrogen and methane absorption upon a change in the methane mixing ratio primarily accounts for such tight combined constraint diagrams. As the methane mixing ratio increases, hydrogen lines require an increase in the model led hydrogen column abundance (i. e, an increase in bottom cloudtop pressure, P_{cld}) to preserve the model led equivalent width (*c.f.*, panel (a) of Figure 5). This is primarily because the increase in background tropospheric methane gas absorption in and around the H_2 line reduces the effective depth of the atmosphere, thus reducing the hydrogen line equivalent width. On the other hand,

a typical curve-of-growth is found for the methane line: As $f_{CH4,t}$ increases, P_{cld} decreases to preserve he equivalent width.

FIGURE 6

in our analysis, such coupled constraint diagrams as shown in Figure 6 were derived for τ_{H} ranging from 0.1 to 0.8, ϖ_{H} covering 0.7 to 1.0, and f_{eH2} ranging from 0.0 (normal H_2) to 1.00 (equilibrium H_2). For all lines, as τ_{H} increases, P_{cld} also increases to preserve the equivalent width. (*c.f.* panels (a) and (c) of Figure 6). It is found that the geometric albedo near the S(0) line then places significant additional constraints on viable (P_{cld}, $f_{CH4,t}$) solutions for large τ_{H}, effectively limiting P_{cld} to a maximum of 4.2 bars where $f_{CH4,t}$ is approximately 0.017.

The standard dev ation between the best fit }12 4-O S(1) model and the observed line profile can be used to constrain τ_{H} and ϖ_{H}. We find that the best combination is of these parameters is $\tau_{H} = 0.40$ and $\varpi_{H}. = 0.90$ (i.e., panel (b) of Figure 6). Overall, we find constraints on P_{cld} of $3.2_{-0.3}^{+1.0}$ bar and $f_{CH4,t} = 0.016_{-0.005}^{+0.007}$ over the full range of viable τ_{H}, ϖ_{H}, and f_{eH2}.

FIGURE 7

Figure 7 shows constraints on the *ortho/para* hydrogen distribution for the nominal $f_{CH4,t}$ solutions of Figure 6. The mini mum f_{eH2}. varies little between the various diagrams, indicating that a minimum f_{eH2} of 0.85 as a hard cons raint. The nominal value of 1.0 means that equilibrium hydrogen is the best solution for Uranus.

IV.C Neptune,

FIGURE

Results of a similar analysis of (P_{cld}, $f_{CH4,t}$ and the *ortho/para* hydrogen distribution for Neptune are shown in Figures 8 and 9. FIGURE Here, the recent analysis of Baines and Hammel (1 994) allows a much narrower range of methane haze opacities to be considered than is the case. for Uranus. We find that $f_{CH4,t}$ is limited to 0.016 - 0.027 and P_{cld} constrained to 3.46 - 4.47 bars, with .nominal values of $f_{CH4,t}$ = 0.022 and P_{cld} = 3.8 bars. The minimum f_{eH2} is 0.89, with a nominal value of 1.0 denoting that equilibrium hydrogen is the best solution for Neptune as well as for Uranus.

V, DISCUSSION

The smaller line strengths and pressure shift coefficients used here compared to previous studies result in a significant increase in the calculated depth of the visible atmosphere and a concomitant reduction in the tropospheric methane mixing ratio for both Uranus and Neptune. In particular, we find the cloud top marking the bottom of the visible atmosphere lies approximately 0.5 bars deeper down in the atmospheres of both planets compared to the previous analyses of Baines and Bergstralh (1986; Uranus) and Baines and Smith (1990; Neptune). The tropospheric methane mixing ratio is reduced by about 30% for both planets. The value found in this' investigation for Neptune, $f_{CH4,t} = 0.022\ ^{+0.005}_{-0.006}$ is in good agreement with the value Of $f_{CH4,t}$ = 0.023 estimated by the Voyager Radio Occultation Experiment (Lindal, 1992). Given the disparate ways $f_{CH4,t}$ 'as

derived (directly from spectroscopic absorption here, indirectly from the pressure level at which a putative methane condensate layer was inferred by Voyager), the similarity of results is remarkable. On the other hand, the low methane mixing ratio found for Uranus $f_{CH4,t} = 0.016^{+0.007}_{-0.005}$ barely overlaps the Voyager Radio Occultation Experiment result (again, $f_{CH4,t} = 0.023$; Lindal *et al.*, 1987).

FIGURE 1(

The elemental carbon-to-hydrogen ratio implied by $f_{CH4,t}$ can be compared to that of the Sun to place constraints on planetary formation scenarios. Figure 10 shows the planetary enhancement in C/H relative to that of the Sun for all the Major Planets. As a function of orbital distance, C/H increases monotonically, thus implying a similar steady increase in the proportion of planetary material derived from condensed, carbon-containing solids in the outer solar system beyond Jupiter and a concomitant decrease in the contribution of nebulae gases. (quantitative constraints on the amount of solid material contributed by carbon-bearing planetesimals to Uranus and Neptune during their early stages of formation can be derived from the planetary formation theory of Bodenheimer and Pollack (1 986) and Pollack *et al.* (1 986). As shown in Figure 11, our data coupled with this theory indicates that at least 2.8% of the carbon in the outer solar system near the orbit of Uranus was originally sequestered in planetestimals, and at least this same percentage of carbon-containing planetesimals was eventually incorporated in the forming Uranian envelope during the planet's early format ve stages. Further out from the Sun, this percentage

FIGURE

figure increases to at least 5% near the orbit of Neptune, as shown in Figure 12. FIGURE

As shown in Figure 13, our finding that molecular hydrogen in FIGURE local thermodynamic equi ibrium fits best the observational data for both Uranus and Neptune s in contrast to Jupiter where at least 5% of the hydrogen s not in equilibrium (Conrath and Gierasch, 1984). This result may not be unexpected given the extended relatively-cold troposphere of these outer worlds (Smith, 1978) and, in the case of Uranus, the lack of an internal heat source. For Neptune, the presence of a large internal heat source may power convective dynamics which conceivably could transport air parcels from the relatively-warm interior in relatively-short timescales, thus perhaps leading to an expectation of un-equilibrated hydrogen. However, the conventional equilibration time of - 3 years may be circumvented by catalytic processes (*e.g.*, Massie and Hunten, 1982). Thus the presence of equilibrium hydrogen as reported here does not necessarily preclude active convective processes within the troposphere of the outermost Major Planets.

ACKNOWLEDGMENTS

The work described in this paper was carried out by the Jet Propulsion laboratory, Pasadena, California, under contract with the National Aeronautics and Space Administration, with support from the Neptune Data Analysis Program and the Planetary Atmospheres Discipline, NASA office of Space Sciences and Applications.

FIGURE CAPTIONS

Figure 1. Uranus: Nominal model structure. Shaded boxed numbers show nominal values derived in this study. These include the tropospheric methane mixing ratio ($f_{CH4,t}$), the *ortho/para* hydrogen distribution (f_{eH2}, the fraction of hydrogen in thermodynamic equilibrium), the pressure of the cloudtop marking the bottom of the visible atmosphere (P_{cld}), the cloud single-scattering albedo (ϖ_{cld}), and the methane haze opacity (ϖ_H) and optical depth (τ_H). Other adopted parameters for various haze and cloud layers are also depicted. I hydrocarbon haze layers extend from the upper stratosphere to the tropospheric methane haze near 1.3 bars. Number densities, particle modal radii (<r>), and condensation levels of primary upper-level haze constituents (diacetylene, C_4H_2; acetylene, C_2H_2; and ethane, C_2H_6) are from Pollack *et al.* (1987). The real refractive index (n_r) of the primary constituent is chosen for each hydrocarbon haze layer above the tropospheric methane haze. The imaginary refractive index is set to 1.00 (conservative scattering). The methane hazetop is assumed situated at the level reported by the Voyager radio occultation experiment (Lindal *et al.*, 1987), while its bottom is assumed located at the methane condensation temperature. Double Henyey-Greenstein particle phase function parameters (g_1, g_2, f]) for the methane haze and bottom cloud layers are from Rages *et al.* (1 991). The thermal profile is that of Lindal *et al.* (1987),

Figure 2. Neptune: Nominal model structure. Shaded boxed quantities show nominal parameters derived in this study. Other atmospheric parameters are from the nominal structure reported by Baines and Hammel (1994), consistent with Voyager imaging and radio occultation results and ground-based imagery. Stratospheric condensation levels of various hydrocarbons and relative weighting of stratospheric column number densities are from Romani *et al.* (1989, 1993). The real component of the refractive index (n_1) for the primary constituent (first listed) is used for each of these stratospheric aerosol layers. Double Henyey-Greenstein particle phase function parameters (g_1, g_2, f) for the methane haze and bottom cloud layers are from Pryor *et al.* (1992) The thermal profile is from Voyager measurements reported by Tyler *et al.* (1989).

Figure 3. Modelled vs observed line profiles for various temperature indices of pressure broadening (γ_{PB}). For both S(0) and S(1) lines, standard deviations (σ) are 30-50% less for α_{PB} = 0.75 than for temperature index α_{PB} = 0.32. These profiles pertain to the nominal atmospheric structure derived in this work: $f_{CH4,t}$ = 0.016, P_{cld} = 3.13 bars for a methane haze opacity τ_H = 0.4 and methane haze single scattering albedo ϖ_H = 0.90.

Figure 4, Standard deviation (σ) vs cloudtop pressure (P_{cld}) for various room-temperature pressure shift and broadening coefficients and pressure-broadening temperature indices (α_{PB}). Over the range of plausible room-temperature coefficients derived by Ferguson *et al.*

(1993), the upper limit ("max Ferg. values") pressure broadening and pressure shift values produce the best fits. Temperature index of 0.75 is superior to 0.32 for both the 4-O S(1) and S(0) lines over all pressures.

Figure 5. Uranus: individual constraints on deep-atmosphere methane molar fraction ($f_{CH4,t}$) and cloud top pressure (P_{cld}) imposed by the equivalent widths of various H_2 4-O quadrupole and 68 18.9-A CH_4 lines and the geometric albedoes of nearby continua. Hydrogen equivalent widths observed by Trauger and Bergstralh (1 981), the methane line equivalent widths determined by Baines *et al.* (1983), and continuum observations of Neff *et al.* (1984, 1985) place significant constraints on these tropospheric parameters. Case shown assumes methane haze cloud opacity of 0.40 and single-scattering al bedo Of 1.00. Panel (a): constraints from H_2 4-O S(1) line equivalent width (shaded nearly-vertical curves) restrict $P_{cld} > 2.6$ bar. Maximum $f_{CH4,t}$ determined from the geometric albedo near the S(1) wavelength (here denoted as the "1/F limit") restricts $f_{CH4,t} < 0.055$, Panel (b): H_2 4-O S(0) line indicates slightly greater pressures; continuum geometric albedo implies $f_{CH4,t} < 0.025$. Panel (c): 6818.9-A methane line equivalent width yields $f_{CH4,t}$ vs P_{cld} behavior nearly orthogonal to that displayed by H2 quadrupole lines depicted in Panels A and *13*.

Figure 6 Uranus: Combined constraints on the deep-atmosphere methane molar fraction ($f_{CH4,t}$) and cloudtop pressure (P_{cld}). Solutions are depicted for two values of the methane haze opacity (Panels (a) and (b): $\tau_H = 0.4$; Pane] (c), $\tau_H = 0.6$) In each panel, three sets of constraints, one set for each of the H2 S4 (1) and S4 (0) lines and another for the 681 8.9-A line (*c.f.* Figure 5) are superimposed, depicting the combined constraints on solutions which simultaneously satisfy all the observed constraints. In each panel, the range of values satisfying all data sets simultaneously is the clear region surrounded by shaded regions and shaded lines. (The shaded region itself indicates solutions which simultaneously satisfy both the hydrogen quadrupole equivalent widths, but not other constraints such as the CH_4 line equivalent width or geometric albedoes). Panels (a) and (b): constraints assuming CH_4 haze optical depth τ_H = 0.4. Pane] (a) is for a conservatively-scattering haze (ϖ_H of 1.0); Panel (b) is for a haze sing] c-scattering albedo ϖ_H = 0.9. P_{cld} is constrained to 2.95 - 3.84 bars over this range of ϖ_H; $f_{CH4,t}$ is limited to = 0.012 - 0.020. Pane] (c): a higher CH_4 haze opacity (τ_H = 0.6) results in a deeper cloudtop (P_{cld} descends to the 3.3 - 4.2 bar region), and a greater methane molar fraction ($f_{CH4,t}$ = 0.015 - 0.023). In each panel, a nominal solution is shown (open circle with dot), defined as the solution which simultaneously fits the nominal equivalent widths of the 681 8.9-Å and H_2 4-O S(I) lines (dashed curves). Standard deviations (numbers) between the observed and modelled H_2 4-0 S(1) line profiles are depicted for the nominal S(1) equivalent width curves. Standard deviations slightly favor the τ_H =

0.4, $\varpi_{H} = 0.9$ solution, indicating nominal values for this study of $f_{CH4,t} = 0.016$, $P_{cld} = 3.13$ bars.

Figure 7 Uranus: H_2 *ortho/para* (distribution determined from 4-O S(0) and S(1) equivalent widths. For each line, cloudtop pressures are depicted (abscissa) which satisfy the observed quadruple equivalent widths over a range of f_{eH2}, the fraction of H_2 in local thermodynamic equilibrium. in each panel - which together span the nominal range of CH_4 molar fractions, methane haze opacities, and methane haze single-scattering al bedoes shown in Figure 6 - only relatively large values of f_{eH2} satisfy both lines simultaneously, as depicted by the cross-hatched area in each panel. Final value for $f_{CH4,t}$ derived in this study, $f_{CH4,t} = 0.016^{+0.007}_{-0.005}$ restricts $f_{eH2} > 0.85$.

Figure 8 Neptune: Combined constraints on deep-atmosphere methane molar fraction ($f_{CH4,t}$) and cloud top pressure (P_{cld}) from the equivalent widths of the H_2 quadrupole and the 681 8.9-Å CH_4 lines observed by Smith and Baines (1 990) and Baines *et al.* (1983). As in Figure 6, clear region surrounded by shaded regions and lines shows range of values satisfying both H_2 and CH_4 data sets, with $f_{CH4,t}$ limited to 0.016 - 0.027 and P_{cld} constrained to 3.46 - 4.47 bars. Nominal value (circled) is $f_{CH4,t} = 0.022$ and $P_{cld} = 3.8$ bars.

Figure 9. Neptune: 112 *ortho/para* distribution determined from 4-O S(O) and S(1) equivalent widths. As with Uranus (Figure 8), only relatively large values of f_{eH2} satisfy both lines simultaneously, as depicted by the cross-hatched area in each panel. Final value for $f_{CH4,t}$ derived in this study, $f_{CH4,t} = 0.022^{+0.006}_{-0.005}$ restricts $f_{eH2} > 0.89$.

Figure 10. C/H enhancement from 5 to 30 AU. Carbon elemental abundances compared to that observed in the Sun by Lambert (1 978) are depicted from this work (open circles) and from others. C/H increases monotonically with solar distance beyond 5 AU, indicating a concomitant increase in the proportion of solid carbon-bearing planetesimal material contributing to planetary formation beyond Jupiter.

Figure 11. Uranus: Theoretical constraints on the amount of condensed carbon delivered by planetesimals during the early stages of planetary formation. The enhanced carbon abundance observed in Uranus compared to that observed in the Sun indicates that a significant amount of carbon was captured by Uranus through the accretion of carbon-bearing planetesimals during the early stages of the planet's evolution, that is, prior to the core's reaching the critical mass for runaway gas accretion (*c.f.* Pollack *et al.*, 1986). Panel (a): 'l'he observed limits on carbon enhancement (relative to that of the Sun) derived in this study are shown against theoretical enhancements derived by Pollack *et al.* (1986). In this plot, the abscissa (α_c) is the fraction of carbon sequestered in condensed

material in the outer solar nebulae during the early stages of planetary formation. Various theoretical curves are shown, pertaining to different values of β_C, which denotes the mass fraction of carbon-containing planetesimals that dissolved in the forming envelope of Uranus and was eventually well-mixed throughout the envelope. Panel (b) shows solutions in exe- β_C space derived from panel (a). Curves are nearly constant in the product $\alpha_C\beta_C$. Minimum $\alpha_C\beta_C$ limit of 0.028 indicates that at least 2.8% of the carbon in the outer solar system was originally sequestered in planetesimals near the Uranian orbit, and that at least a similar fraction of carbon-containing planetesimals was eventually incorporated in the young Uranian envelope.

Figure *12*. Neptune: Theoretical constraints on the amount of condensed carbon delivered by planet esimals during the early stages of planetary formation, Same as in Figure 11, except for Neptune. Mini mum $\alpha_C\beta_C$ limit of 0.050 is nearly twice that of Uranus, indicating that a significantly higher percentage of solid carbon material near Neptune's orbit eventually was incorporated into the planet.

Figure 13. The *ortho/para hydrogen* distribution in the outer Solar System. Local thermodynamic equilibrium fits best the observational data for both Uranus and Neptune (open circle), in contrast to Jupiter where at least 5% of the hydrogen is not in equilibrium.

REFERENCES

Atreya, S. K. and P. N. Romani. 1985. Photochemistry and clouds of Jupiter, Saturn, and Uranus. in *Recent Advances in Planetary Meteorology*, ed. G. E. Hunt (Cambridge Univ. Press), pp. 17-68,

Baines, K. H. 1983. Interpretation of the 681 8.9-Å methane feature observed on Jupiter, Saturn, and Uranus. *Icarus* 56, 543-559.

Baines, K. 11., and J. T. Bergstralh. 1986. The structure of the Uranian atmosphere: constraints from the geometric albedo spectrum and H_2 ant] CH_4 line profiles. *Icarus* 65, 406-441.

Baines, K. H., and H. B. Hammel. 1994. Clouds, hazes, and the stratospheric methane abundance in Neptune. *Icarus*, in press.

Baines, K. H., W. V. Schempp, and W. H. Smith. 1983. High-resolution observations of the 681 5-Å band of methane in the major planets. *Icarus* 56, 534- 542.

Baines, K, H. and W. H. Smith 1990. 'l'he atmospheric structure and dynamical properties of Neptune derived from ground-based IUE spectrophotometry. *Icarus* 85, 65-108.

Baines, K. H., W. H. Smith, and C. Alexander. 1989. Spatial and temporal variations of NH_3 abundance and cloud structure in the Jovian troposphere derived from CCD/Coudé observations. In *Time Variable Phenomena of the Jovian System*. (Belton, Rahe, and West, Eds), NASA S1)-494, 363-370.

Bergstralh, J. T., J. S. Margolis, and J. W. Brault. 1978. Intensity and pressure shift of the H_2 (4,0) S(1) quadruple line. *Astrophys. J. Lett. 224,* 39 - *41.*

Birnbaum, G. 1967. Advances in Chemical Physics, Intermolecular Forces (J. O. Hirschfelder, Ed), Vol. 12. Interscience, New York.

Bodenheimer, P., and J. B. Pollack. 1986. Calculations of the accretion and evolution of giant planets: The effects of solid cores. *Icarus* 67, 391 - 408.

Bragg, S. L. 1981. *An Experimental Study of Vibrational-Rotational Spectra of Molecular Hydrogen.* Ph.D. thesis. Washington University, St. Louis, Mo.

Bragg, S. I.., J, W. Brault, and W. }1. Smith. 1982, Line positions and strengths in the H_2 quadrupole spectrum, *Astrophys. J. 263,* 999- 1004.

Brault, J. W. and W. H. Smith. 1980. Determination of the H_2 4-O S(1) quadruple line strength and pressure shift . *Astrophys. J.. Lett.* 23s. L177-178.

Cochran, W. D. and W. H. Smith. 1983. Desaturation of H_2 quadruple lines in the atmospheres of the giant planets. *Astrophys. J.* **271**, *859-864.*

Conrath, B. J., D. Gautier, G. F. Lindal, R. E. Samuelson, and W. A. Shaffer. 1991. The helium abundance of Neptune from Voyager measurements. *J. Geophys. Res. 96, 18907* - 18919.

Conrath, B. J. and P. J. Gierasch. 1984. Global variations of the para hydrogen fraction in Jupiter's atmosphere and implications for dynamics on the outer planets. *Icarus* 101, 184 - 204.

Courtin, R., D. Gautier, A. Marten, B. Bézard, and R. Hanel. 1984 The composition of Saturn's atmosphere at northern latitudes from Voyager IRIS spectra: NH_3, PH_3, C_2H_2, C_2H_6, CH_3D, CH4, and the Saturnian D/H isotopic ratio. *Astrophys. J. 287,* 899-916.

Ferguson, D. W., K. Narahari Rae, M. E. Mickelson, and L. E. Larson. 1993. An experimental study of the 4-O and 5-O quadruple vibration rotation bands of H_2 in the visible. *J. Mol. Spec.* 160, 315 - 325,

Galatry, L. *1961*. Simultaneous effect of Doppler and foreign gas broadening on spectral lines, *Phys. Rev.* **122**, 1218 - 1223.

Gautier, D., B, Bézard, A, Marten, J. P. Baluteau, N. Scott, A. Chedin, V. Kunde, and R. Hanel. 1982, The C/H ratio in Jupiter from the Voyager infrared investigation. *Astrophys. J. 257, 901 - 912.*

Giver, L. P. 1978. Intensity measurements of the CH4 bands in the region 4350 Å to 10600 Å. *J. Quant. Spectrosc. Radiat. Transfer* 19, 311 - *322*.

Hammel, H. B., and M. W. Buie. 1987. An atmospheric rotation period of Neptune determined from methane-band imaging. *Icarus* 72, 62-68.

Karkoschka, E., and M, G. Tomasko. 1992. Saturn's upper troposphere 1986 - 1989. *Icarus 97, 161* - 181.

Keffer, C. E. 1985. *High-Resolution Die-Laser Photo-Acoustic Spectroscopy of Visible Wavelengths, Vibrational-Rotational Transitions in Molecules Important to the Study of Planetary Atmosphere*. Ph. D. thesis. Washington University, St. Louis, Mo.

Keffer, C. E., C. P. Conner, and W. H. Smith. 1986. Pressure broadening of methane in the 6190 A and 682.0 Å bands at low temperature. *J. Quant. Spectrosc. Radiat. Transfer* **35**, *495 - 499.*

Lambert, D. L. 1978. The abundances of elements in the solar photosphere - VIII. Revised abundances of carbon, nitrogen, and oxygen *Mon. Not. Roy. Astron. Soc. 192, 249-272.*

Lindal, G. F. 1992. The atmosphere of Neptune: An analysis of radio occultation data acquired with Voyager 2. *Astron. J. 103, 967 - 982.*

Linda], G. F., J. R. Lyons, D. N. Sweetman, V, R. Eshleman, D. P. Hinson, and G. L. Tyler.1 987. The atmosphere of Uranus: Results of radio occultation measurements with Voyager 2. *J. Geophys.. Res.* 92, 14987 - 15001,

Massie, S, T., and D. M. Hunten. 1982. Conversion of *para* and *ortho* hydrogen in the Jovian planets. *Icarus* 49, 213 - 226.

McKellar, A. R. W. 1974. The significance of pressure shifts for the interpretation of H_2 quadrupole lines in planetary spectra. *Icarus* 22, 212-219.

Mizuno, H., K. Nakazawa, and C. Hayashi. 1978. Instability of gaseous envelopes surrounding planetary cores and formation of giant planets. *Prog. Theor. Phys.* 60, 699 - 710,

Neff, J, S., T. A. Ellis, J, Apt, and J. '1'. Bergstralh .1985. Bolometric albedos of Titan, Uranus, and Neptune. *Icarus* 62, 425 - 432.

Neff, J. S., D, C. Humm, J. T. Bergstralh, A. L. Cochran, W. D. Cochran, E. S, Barker, and R, G. Tull. 1984. Absolute spectrophotometry of Titan, Uranus, and Neptune: 3500 - 10500 Å. *Icarus* 60, *221- 235.*

Orton, G. S., M. J. Griffin, P. A. R. Ade, I. G. NoIt, J. V. Radostitz, E. 1. Robson, and W. K. Gear. 1986. Submillimeter and Millimeter Observations of Uranus and Neptune. *Icarus* 67, 289-304.

Poll, J. D. and L. Wolniewicz. 1978. The quadruple moment of the H_2 molecule. *J. Chem. Phys.* J. 68, 3053 - 3058.

Pollack, J. B., M. Podolak, P. Bodenheimer and H. Christofferson. 1986. Planetesimal dissolution in the envelopes of the forming, giant planets, *Icarus* 67, 409 - 443.

Pollack, J. B., K. Rages, S. K. Pope, M. G. Tomasko, P. N. Romani, and S. K. Atreya. 1987. Nature of the stratospheric haze on Uranus: Evidence for condensed hydrocarbons. *J. Geophys. Res.* 92, 15037 - 15065,

Pryor, W. R., R. A. West, K. E. Simmons, and M. Delitsky. 1992. High-phase-angle observations of Neptune at 2650 A and 7500 A: Haze structure and particle properties. *Icarus* 99, 302-317

Rages , K. , J. B. Pollack, M. G. Tomasko, and L. R. Doose. 1991, Properties of scatterers in the troposphere and lower stratosphere of Uranus based on Voyager imaging data. *Icarus 89,* 359 - *376.*

Romani, P. N., and S. K. Atreya. 1989. Stratospheric aerosols from CH_4 photochemistry on Neptune. *Geophys. Res. Lett.* **16**, *941 - 944!*

Romani, P. N., J. Bishop, B. Bézard, ant] S. Atreya. 1993. Methane photochemistry on Neptune: Ethane ant] acetylene mixing ratios and haze production. *Icarus* 106, 442 - 463.

Smith, B. A., L. A. Soderblom, R. Beebe, D. Bliss, J. M. Boyce, A. Brahic, G. A. Briggs, R. H. Brown, S. A. Collins, A. F. Cook, II, S. K. Croft, J. N. Cuzzi, G. E. Danielson, A. P. Ingersoll, T. V. Johnson, *et al.* 1986. Voyager 2 in the Uranian system: imaging science results. *Science* **233**, *43-64,*

Smith, W. H. *1978.* On the *ortho-para* equilibrium of H_2 in the atmospheres of the Jovian planets. Icarus **33**, 210-216.

Smith, W. H. and K. H. Baines. *1990.* H_2 $S_3(1)$ and *S4(1)* transitions in the atmospheres of Neptune and Uranus: observations and analysis. *Icarus* 85, 109 - 119.

Townes, C. H. and A. Schawlow. 1955. ***Microwave Spectroscopy*** McGraw-Hill, New York.

Trafton, L. 1967. Model atmospheres of the major planets. *Astrophys. J. 147, 765-781.*

Trauger, J.T and J. T. Bergstralh. 1981. Asymmetrical profiles of the H_2 4-0 quadrupole lines in the spectrum of Uranus. *Bull. Amer. Astron. Sot.* **13**, *732.*

Trauger, J. '1'., M. E. Michelson, and L. E. Larson. 1978. laboratory absorpt on strengths for the H_2 (4,0) and (3,0) S(1) lines *Astrophys. J. Lett.* 225, 157 - 160.

Tyler, G. L., D. N, Sweetman, J. D. Anderson, S. E. Borutzki, J. K. Campbell, V. R. Eshleman, 1>. 1,. Gresh, E. M. Gurrola, D. P, Hinson, N. Kawashima, E. R, Kursinski, G. S. Levy, G. F. Linda], J. R. Lyons, E. A. Marouf, P. A. Rosen, R. A. Simpson, and G. E. Wood. 1989, Voyager radio science observations of Neptune and Triton. *Science* 246, 1466 - 1473.

FIGURE 1

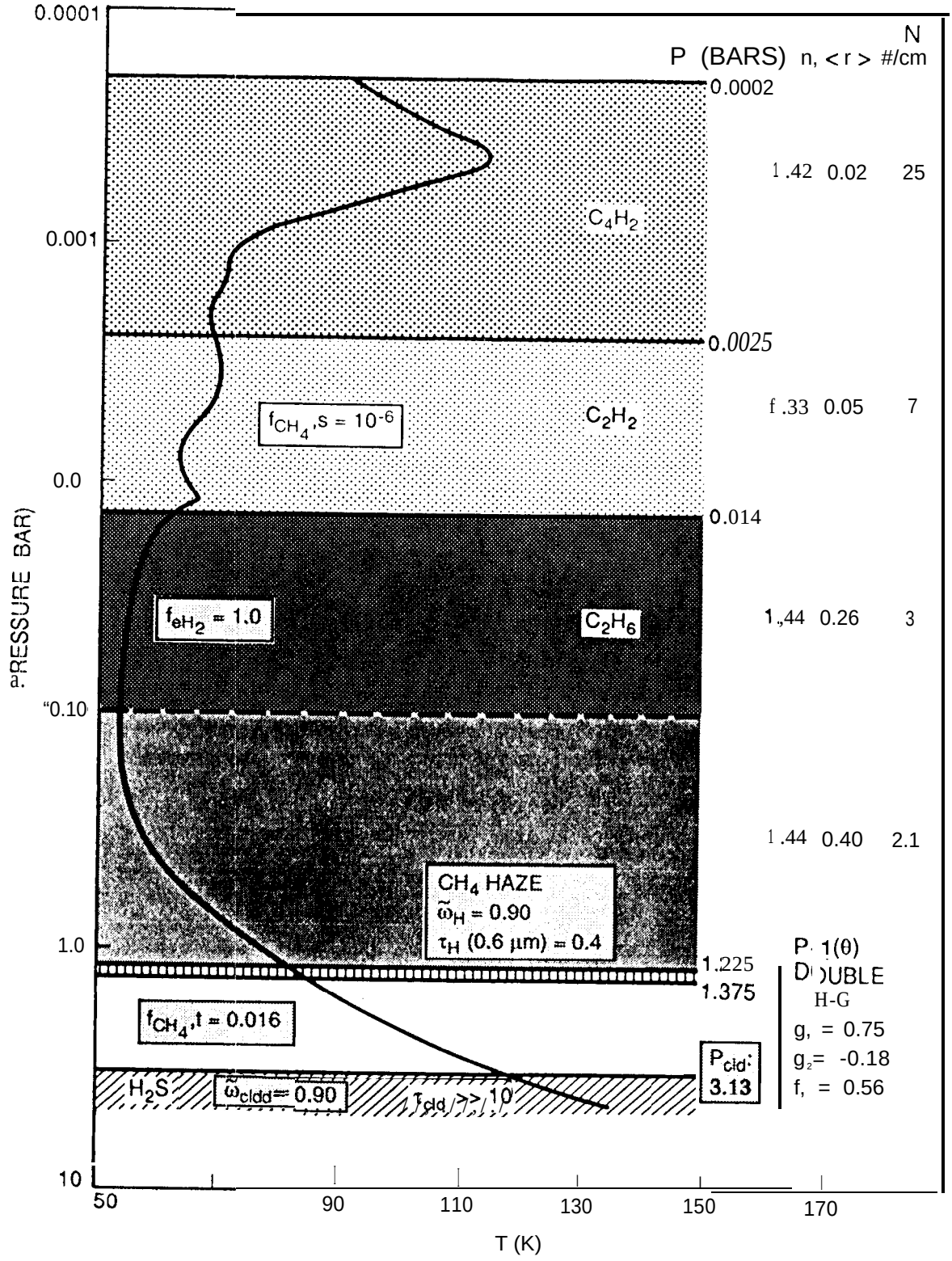
P (BARS)
N
n, < r > #/cm
0.0001
0.001
0.0
0.10
1.0
10
0.0002
0.0025
0.014
1.225
1.375
1.42 0.02 25
f .33 0.05 7
1.44 0.26 3
1.44 0.40 2.1
C4H2
C2H2
C2H6
CH4 HAZE
ω̃H = 0.90
τH (0.6 μm) = 0.4
fCH4,s = 10-6
feH2 = 1.0
fCH4,t = 0.016
H2S
ω̃cldd= 0.90
τcld >> 10
Pcld: 3.13
P 1(θ)
DOUBLE
H-G
g, = 0.75
g2= -0.18
f, = 0.56
50
90
110
130
150
170
T (K)

FIGURE 2

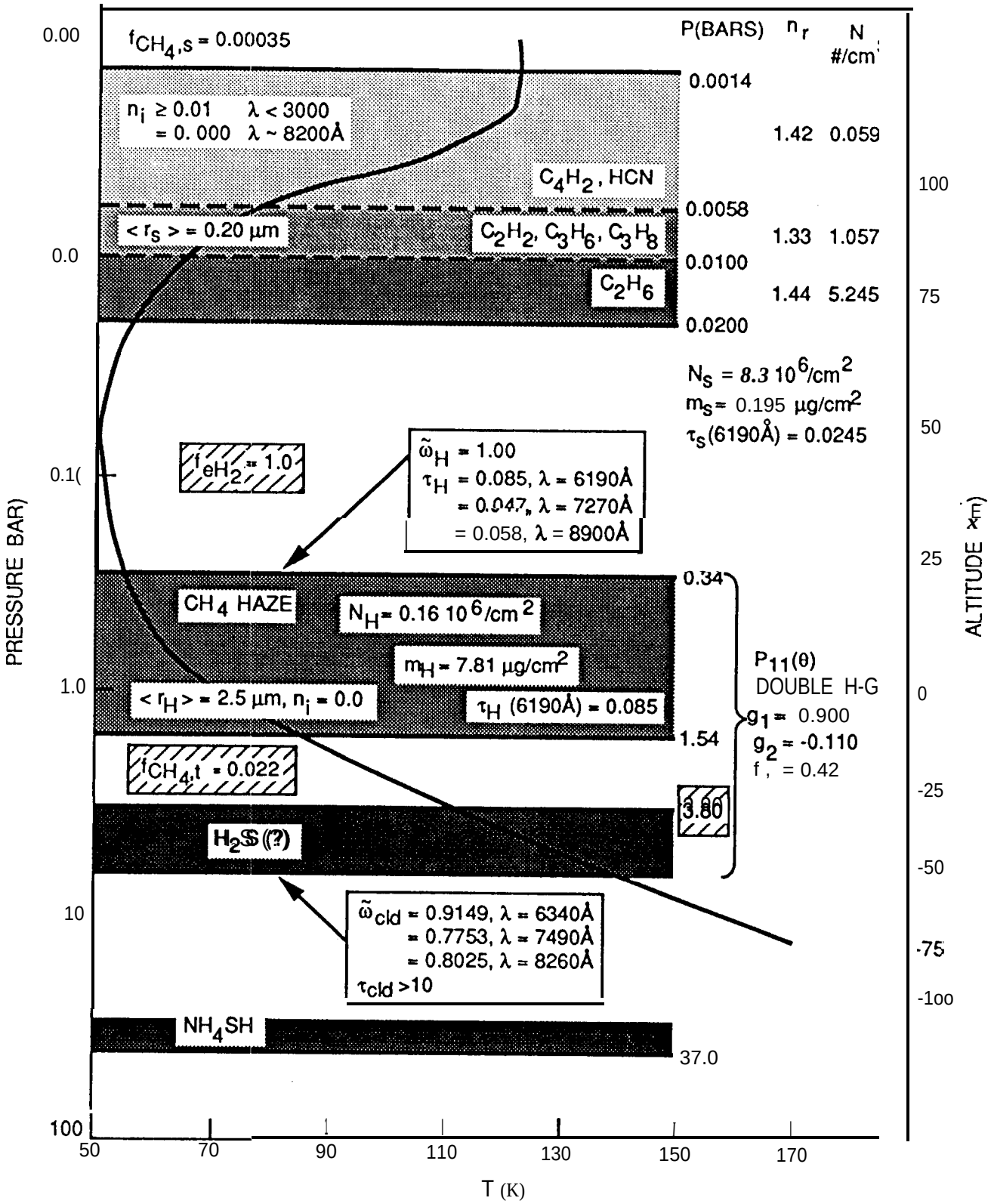
$f_{CH_4,s}$ = 0.00035
P(BARS) n_r N #/cm³
0.0014
$n_i \geq 0.01$ $\lambda < 3000$
= 0. 000 $\lambda \sim 8200$Å
1.42 0.059
C_4H_2, HCN
0.0058
$< r_s > = 0.20\ \mu m$
C_2H_2, C_3H_6, C_3H_8
1.33 1.057
0.0100
C_2H_6
1.44 5.245
0.0200
$N_S = 8.3\ 10^6/cm^2$
m_S = 0.195 µg/cm²
τ_S(6190Å) = 0.0245
f_{eH_2} = 1.0
$\tilde{\omega}_H$ = 1.00
τ_H = 0.085, λ = 6190Å
= 0.047, λ = 7270Å
= 0.058, λ = 8900Å
CH_4 HAZE
$N_H = 0.16\ 10^6/cm^2$
m_H = 7.81 µg/cm²
$< r_H > = 2.5\ \mu m$, n_i = 0.0
τ_H (6190Å) = 0.085
0.34
1.54
$P_{11}(\theta)$
DOUBLE H-G
g_1 = 0.900
g_2 = -0.110
f, = 0.42
$f_{CH_4,t}$ = 0.022
3.80
H_2S (?)
$\tilde{\omega}_{cld}$ = 0.9149, λ = 6340Å
= 0.7753, λ = 7490Å
= 0.8025, λ = 8260Å
τ_{cld} >10
NH_4SH
37.0
0.00
0.0
0.1(
1.0
10
100
PRESSURE BAR)
50
70
90
110
130
150
170
T (K)
100
75
50
25
0
-25
-50
-75
-100
ALTITUDE (km)

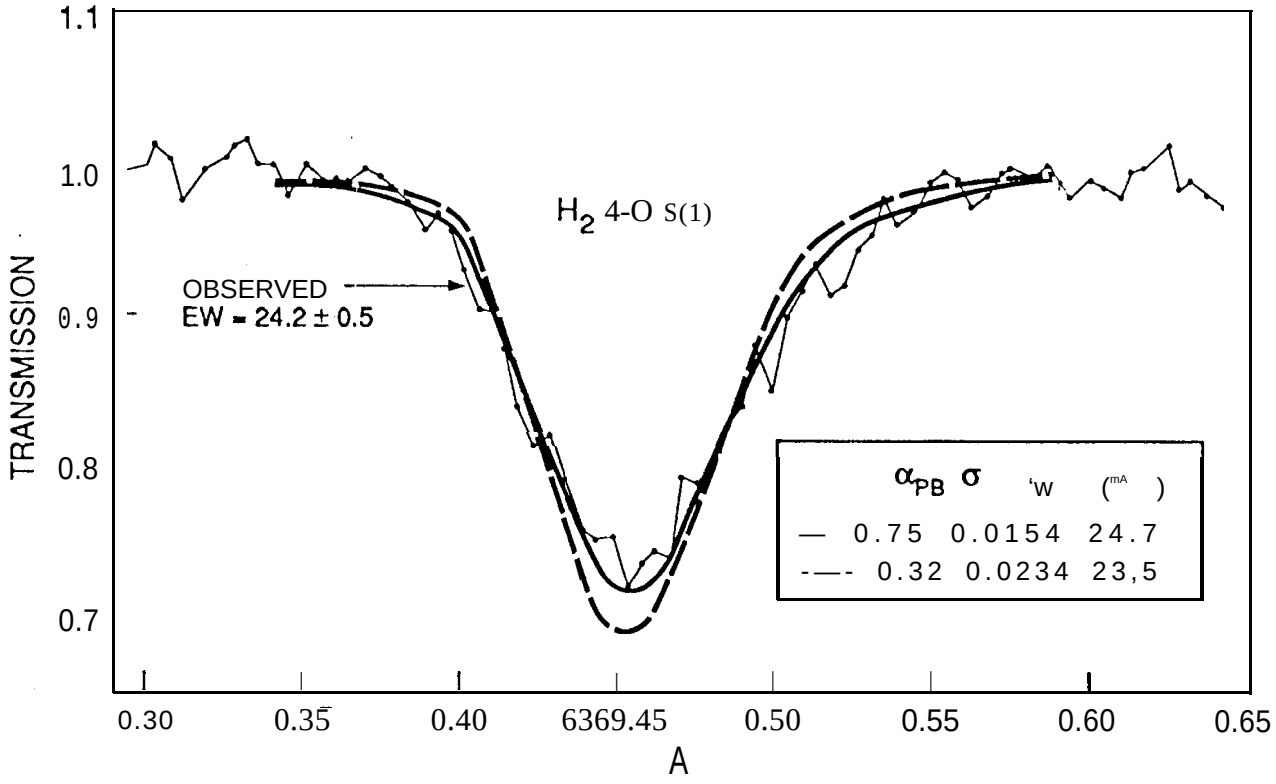
1.1
1.0
0.9
0.8
0.7
TRANSMISSION
H_2 4-O S(1)
OBSERVED
EW = 24.2 ± 0.5
α_{PB} σ 'W (mA)
— 0.75 0.0154 24.7
-—- 0.32 0.0234 23,5
0.30
0.35
0.40
6369.45
0.50
0.55
0.60
0.65
A

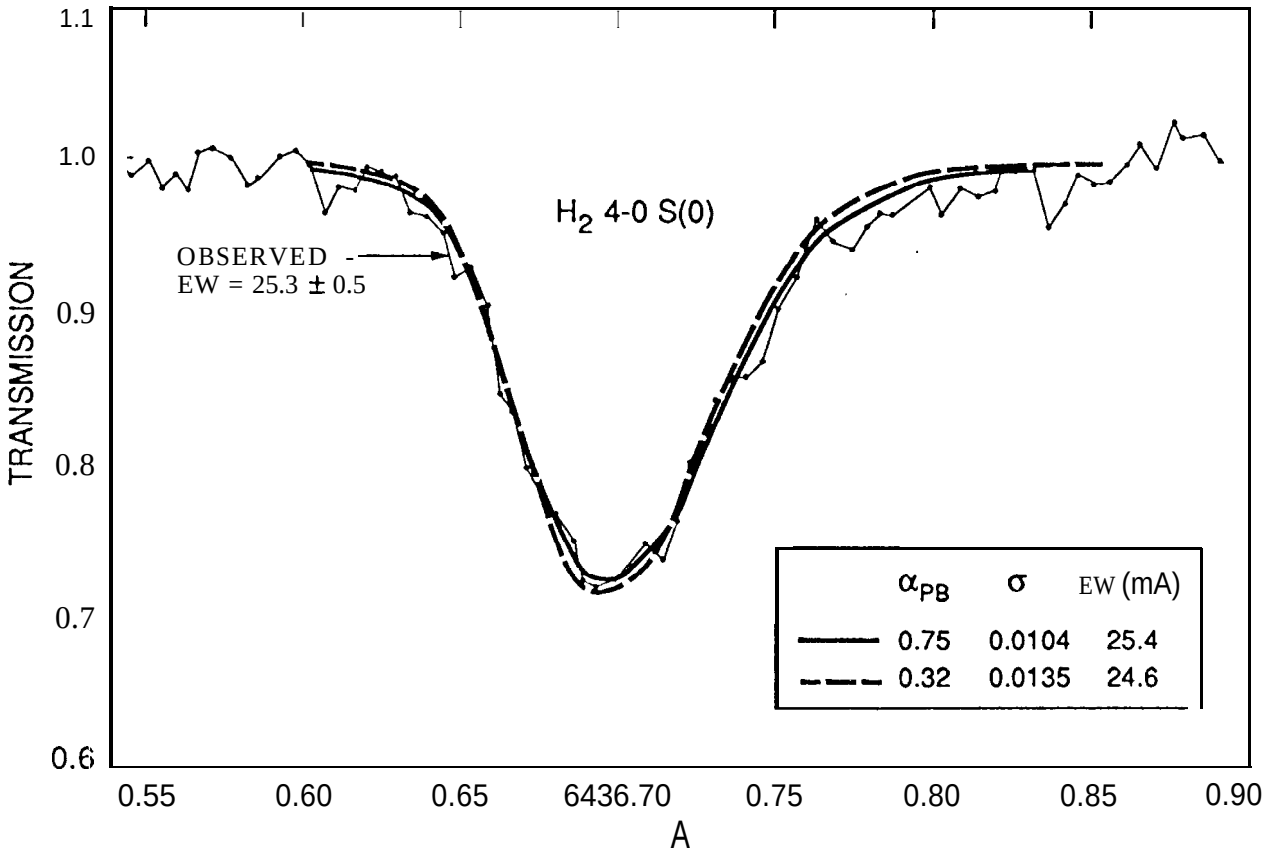
1.1
1.0
0.9
0.8
0.7
0.6
TRANSMISSION
H_2 4-0 S(0)
OBSERVED
EW = 25.3 ± 0.5
α_{PB} σ EW (mA)
0.75 0.0104 25.4
0.32 0.0135 24.6
0.55
0.60
0.65
6436.70
0.75
0.80
0.85
0.90
A

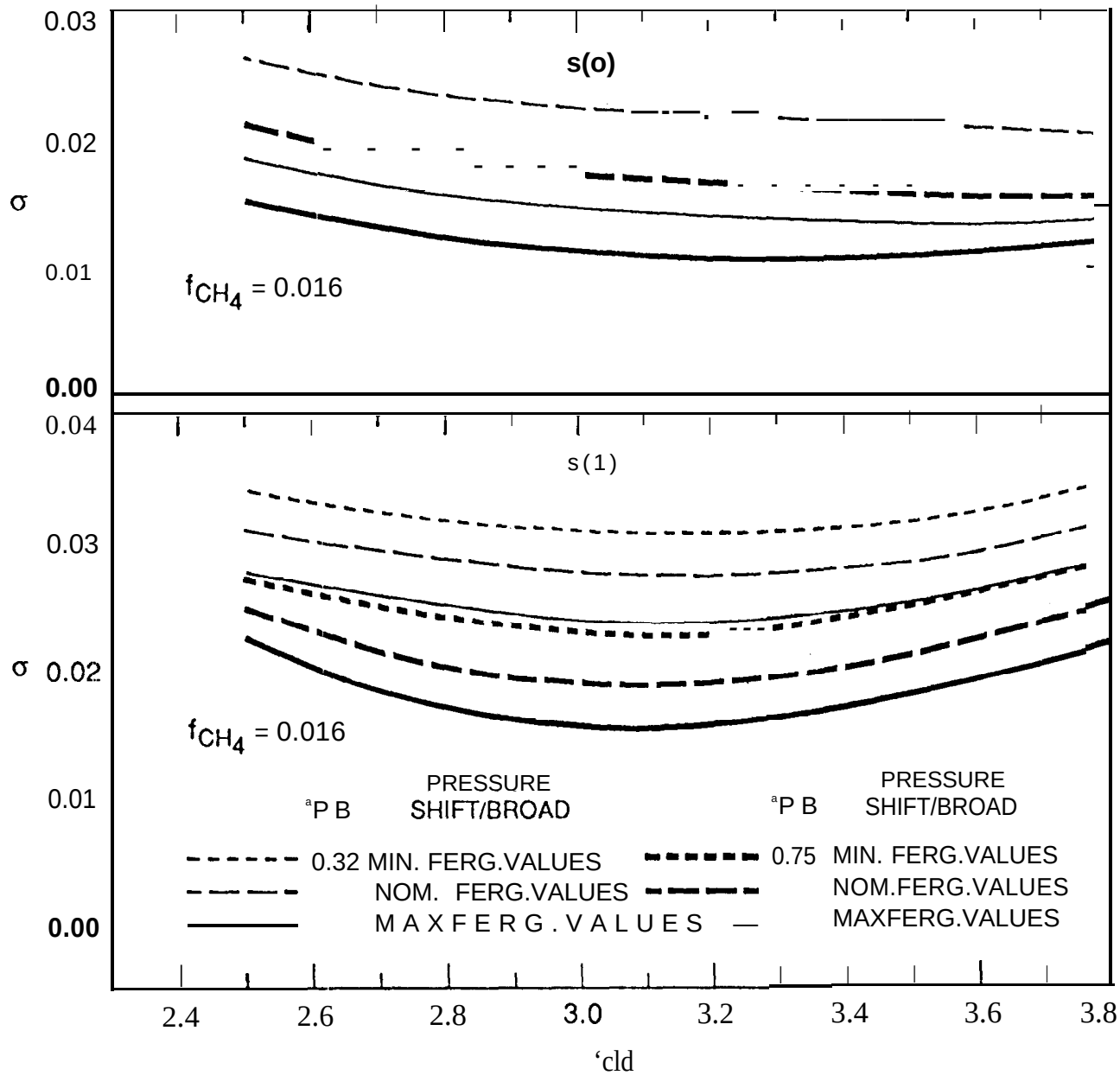
0.03
0.02
σ
0.01
0.00
s(o)
f_{CH_4} = 0.016
0.04
0.03
σ 0.02
0.01
0.00
s(1)
f_{CH_4} = 0.016
PRESSURE SHIFT/BROAD
^{a}P B
0.32 MIN. FERG.VALUES
NOM. FERG.VALUES
MAXFERG.VALUES
PRESSURE SHIFT/BROAD
^{a}P B
0.75 MIN. FERG.VALUES
NOM.FERG.VALUES
MAXFERG.VALUES
2.4
2.6
2.8
3.0
3.2
3.4
3.6
3.8
'cld

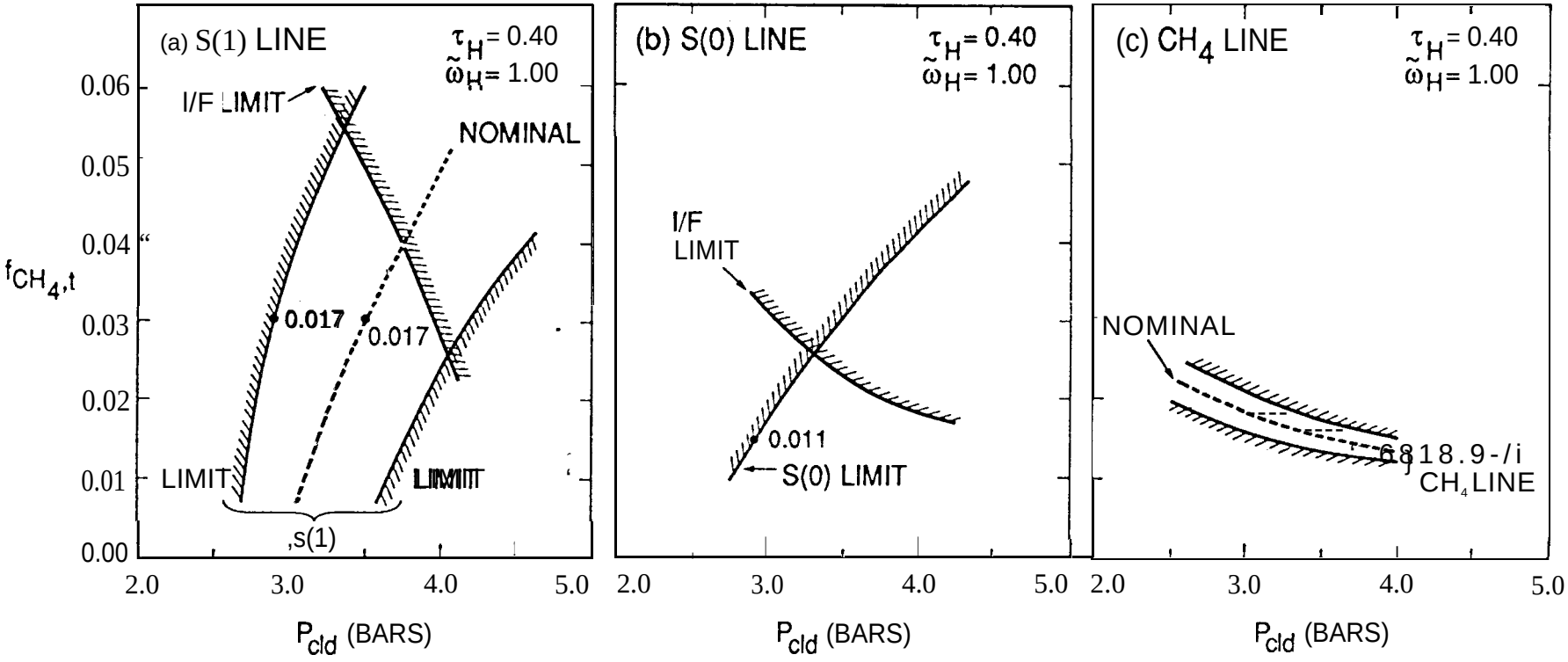
(a) S(1) LINE
τ_H= 0.40
$\tilde{\omega}_H$= 1.00
I/F LIMIT
NOMINAL
0.017
0.017
LIMIT
LIMIT
,s(1)
$f_{CH_4,t}$
0.06
0.05
0.04
0.03
0.02
0.01
0.00
2.0
3.0
4.0
5.0
P_{cld} (BARS)
(b) S(0) LINE
τ_H= 0.40
$\tilde{\omega}_H$= 1.00
I/F
LIMIT
0.011
S(0) LIMIT
2.0
3.0
4.0
5.0
P_{cld} (BARS)
(c) CH_4 LINE
τ_H= 0.40
$\tilde{\omega}_H$= 1.00
NOMINAL
6818.9-/i
CH_4 LINE
2.0
3.0
4.0
5.0
P_{cld} (BARS)

FIGURE 5

FIGURE 6

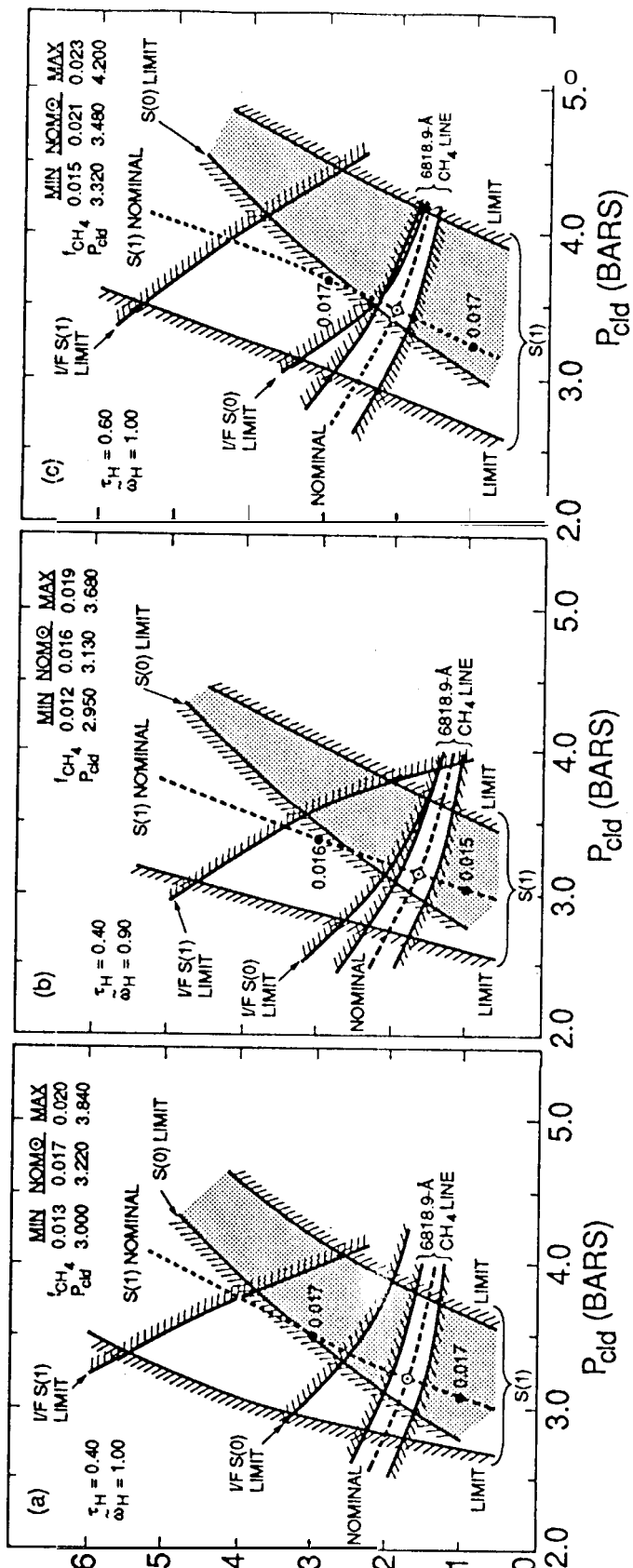
(a)
τ_H = 0.40
$\tilde{\omega}_H$ = 1.00
(b)
τ_H = 0.40
$\tilde{\omega}_H$ = 0.90
(c)
τ_H = 0.60
$\tilde{\omega}_H$ = 1.00
MIN NOM⊙ MAX
f_{CH_4} 0.013 0.017 0.020
P_{cld} 3.000 3.220 3.840
MIN NOM⊙ MAX
f_{CH_4} 0.012 0.016 0.019
P_{cld} 2.950 3.130 3.680
MIN NOM⊙ MAX
f_{CH_4} 0.015 0.021 0.023
P_{cld} 3.320 3.480 4.200
I/F S(1) LIMIT
I/F S(0) LIMIT
S(1) NOMINAL
S(0) LIMIT
NOMINAL
LIMIT
S(1)
6818.9-Å CH_4 LINE
0.017
0.016
0.015
f_{CH_4}, t
P_{cld} (BARS)

FIGURE 7

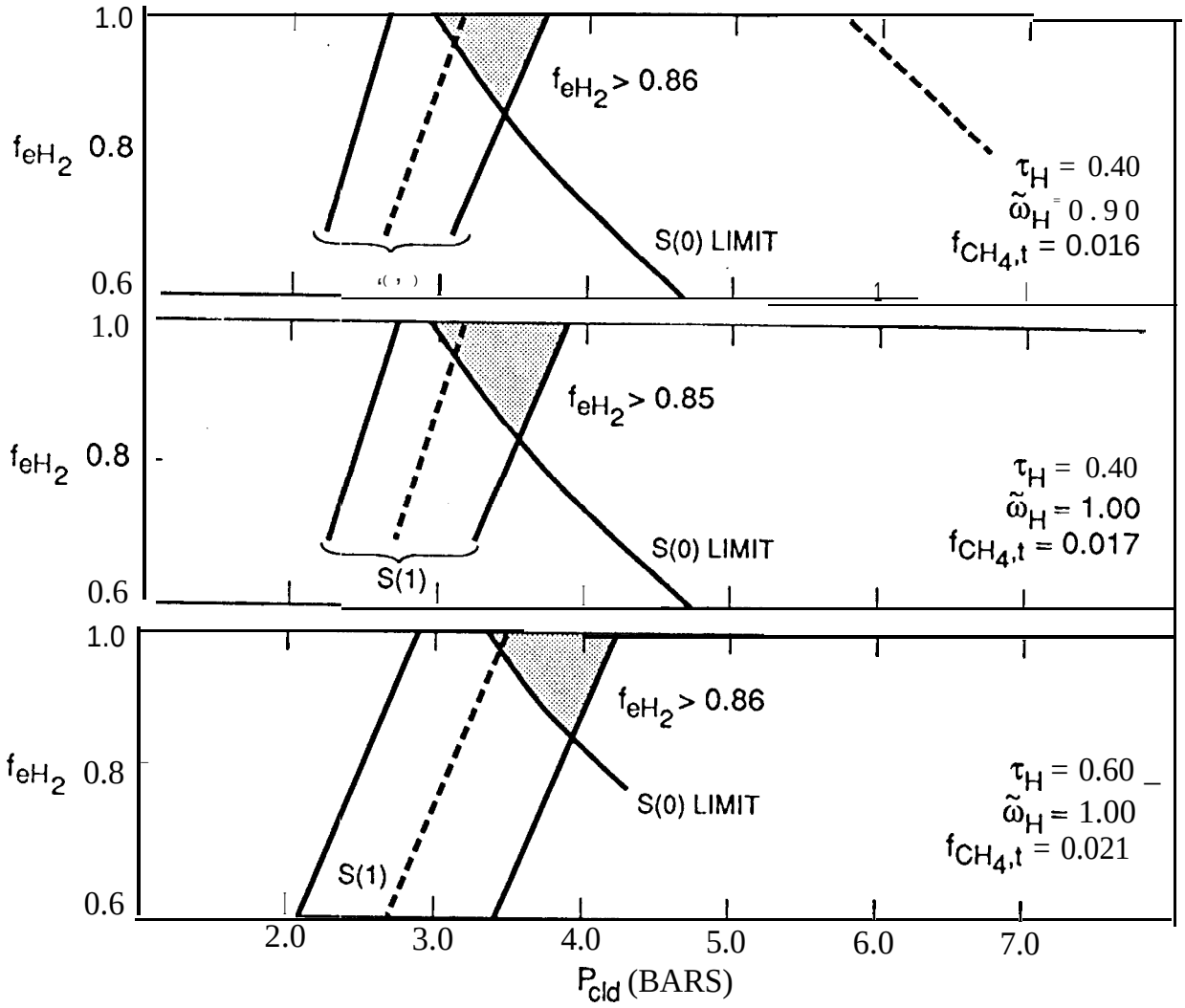
1.0
0.8
0.6
f_{eH_2}
$f_{eH_2} > 0.86$
S(0) LIMIT
S(1)
$\tau_H = 0.40$
$\tilde{\omega}_H = 0.90$
$f_{CH_4,t} = 0.016$
$f_{eH_2} > 0.85$
$\tau_H = 0.40$
$\tilde{\omega}_H = 1.00$
$f_{CH_4,t} = 0.017$
$f_{eH_2} > 0.86$
$\tau_H = 0.60$
$\tilde{\omega}_H = 1.00$
$f_{CH_4,t} = 0.021$
2.0
3.0
4.0
5.0
6.0
7.0
P_{cld} (BARS)

FIGURE 8

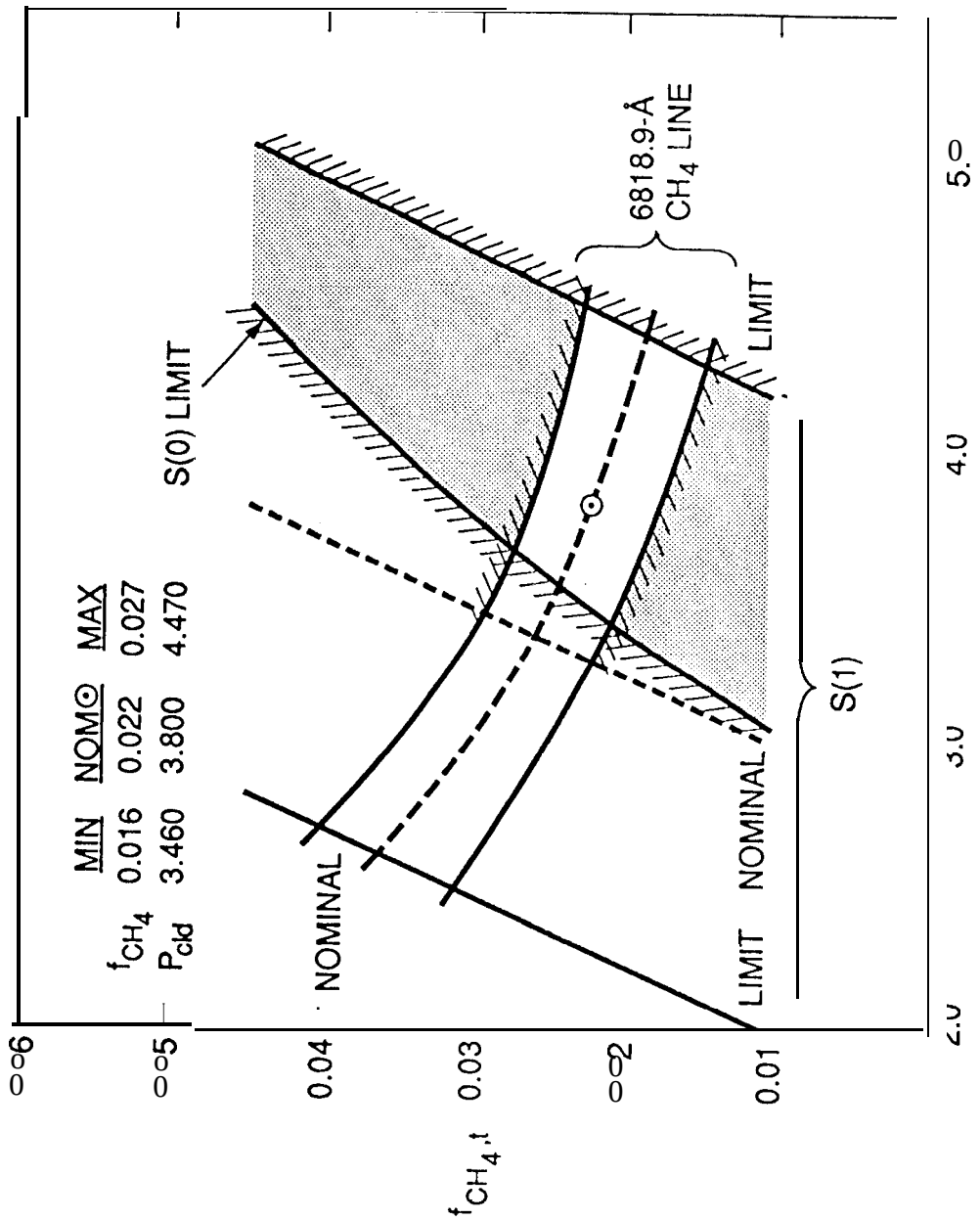
6818.9-Å
CH_4 LINE
S(0) LIMIT
LIMIT
NOMINAL
LIMIT
NOMINAL
S(1)
MIN NOM⊙ MAX
f_{CH_4} 0.016 0.022 0.027
P_{cld} 3.460 3.800 4.470
$f_{CH_4,t}$
P_{cld} (BARS)
0.04
0.03
0.01
4.0
5.0

FIGURE 9

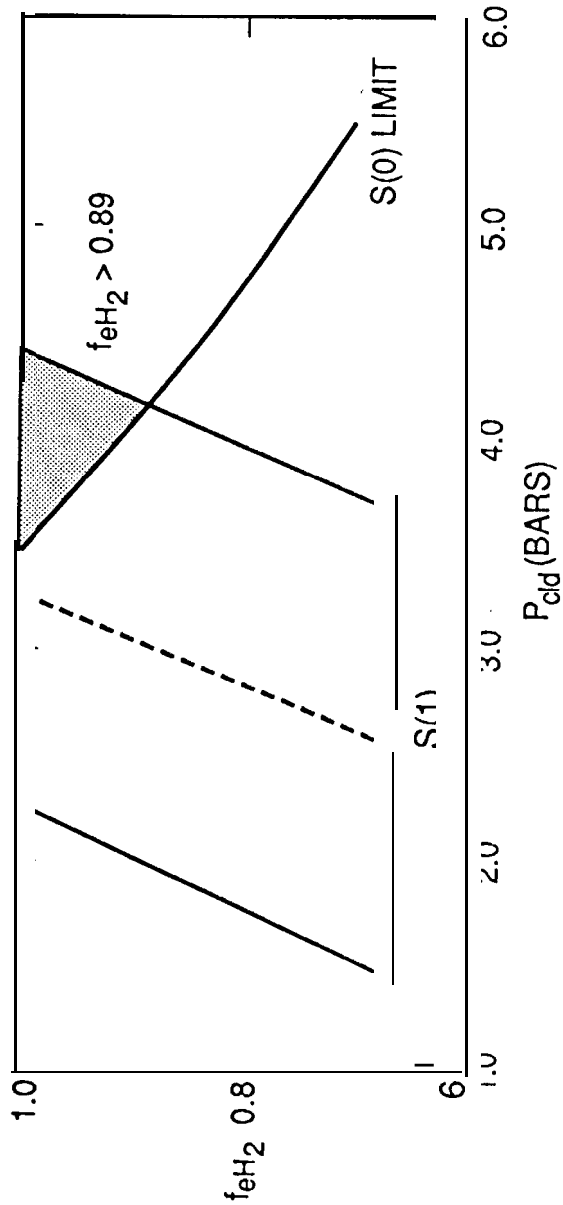

FIGURE 10

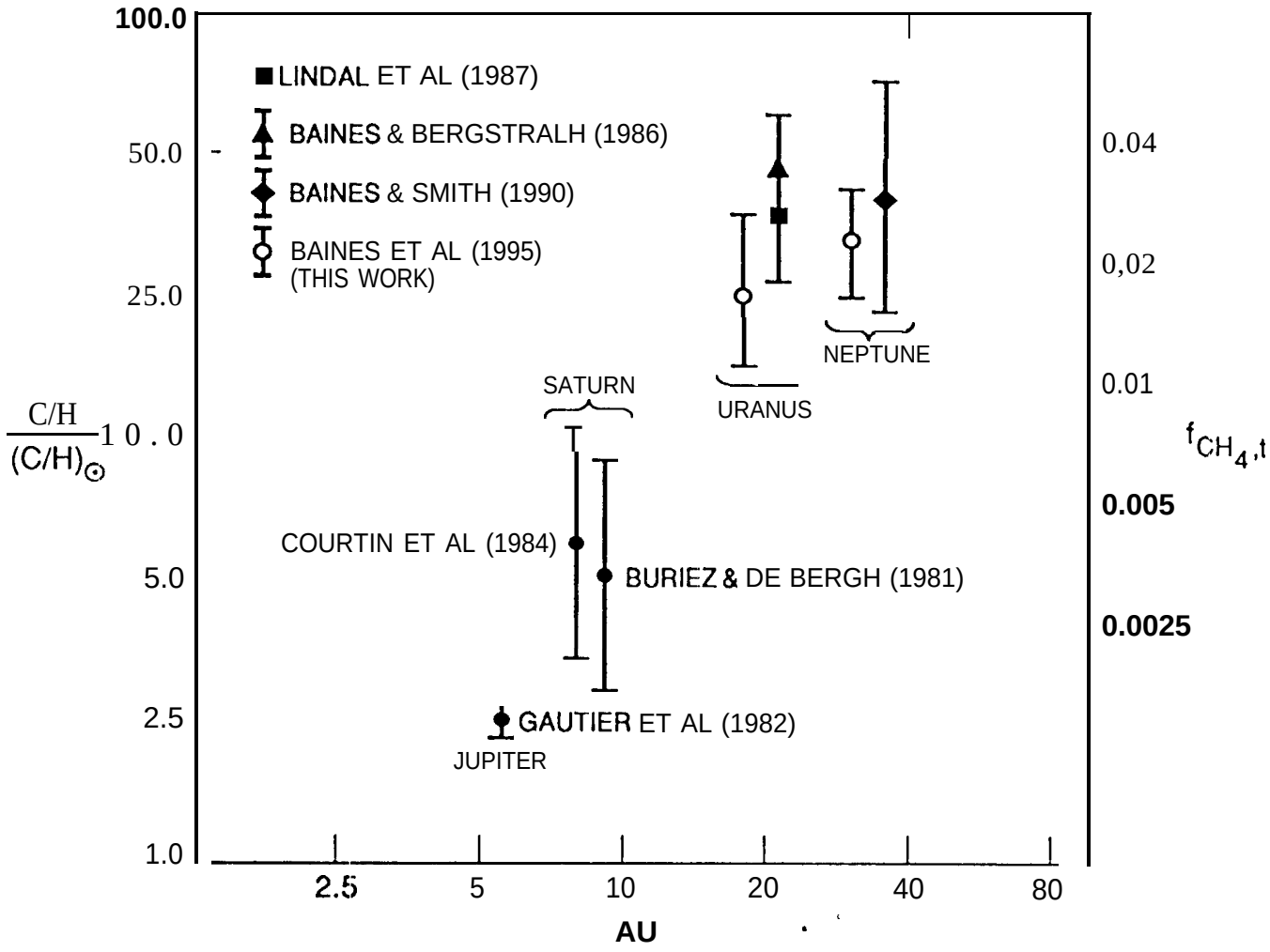
100.0
50.0
25.0
10.0
5.0
2.5
1.0
C/H / (C/H)⊙
LINDAL ET AL (1987)
BAINES & BERGSTRALH (1986)
BAINES & SMITH (1990)
BAINES ET AL (1995)
(THIS WORK)
SATURN
URANUS
NEPTUNE
COURTIN ET AL (1984)
BURIEZ & DE BERGH (1981)
GAUTIER ET AL (1982)
JUPITER
0.04
0,02
0.01
0.005
0.0025
$f_{CH_4,t}$
2.5
5
10
20
40
80
AU

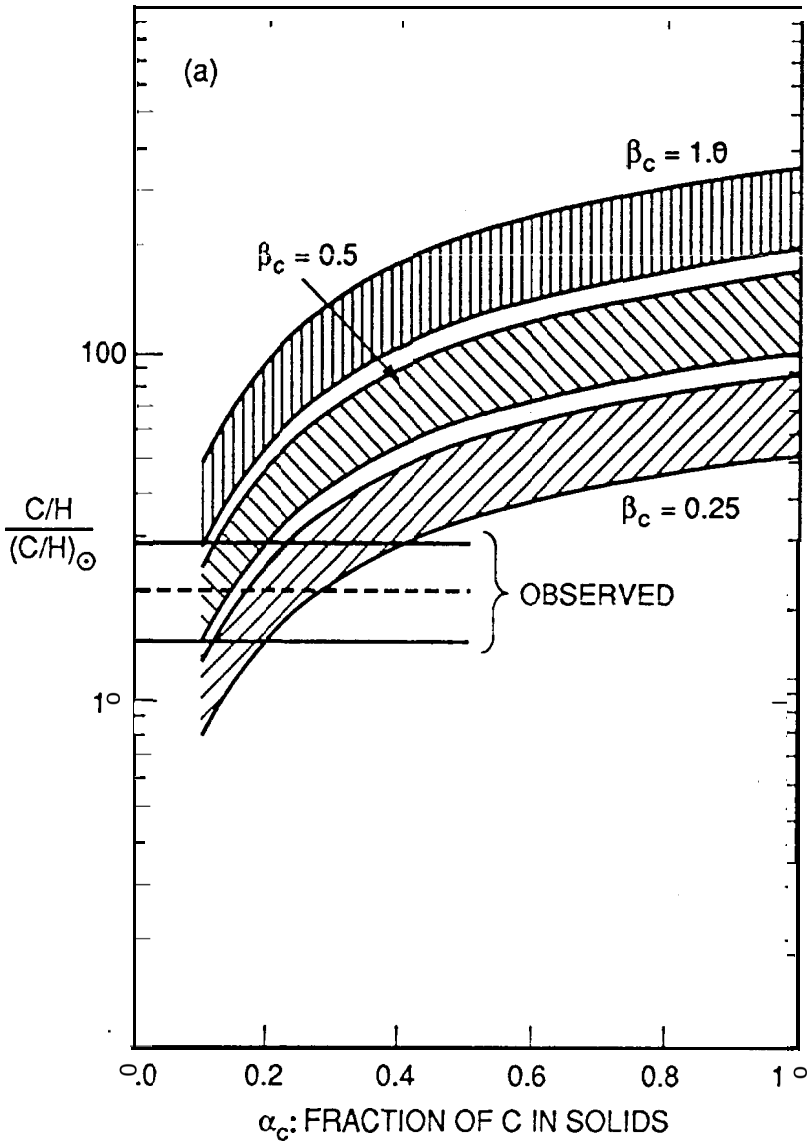
(a)
β_c = 1.0
β_c = 0.5
β_c = 0.25
OBSERVED
100
1°
C/H
(C/H)⊙
°.0
0.2
0.4
0.6
0.8
1 °
α_c: FRACTION OF C IN SOLIDS

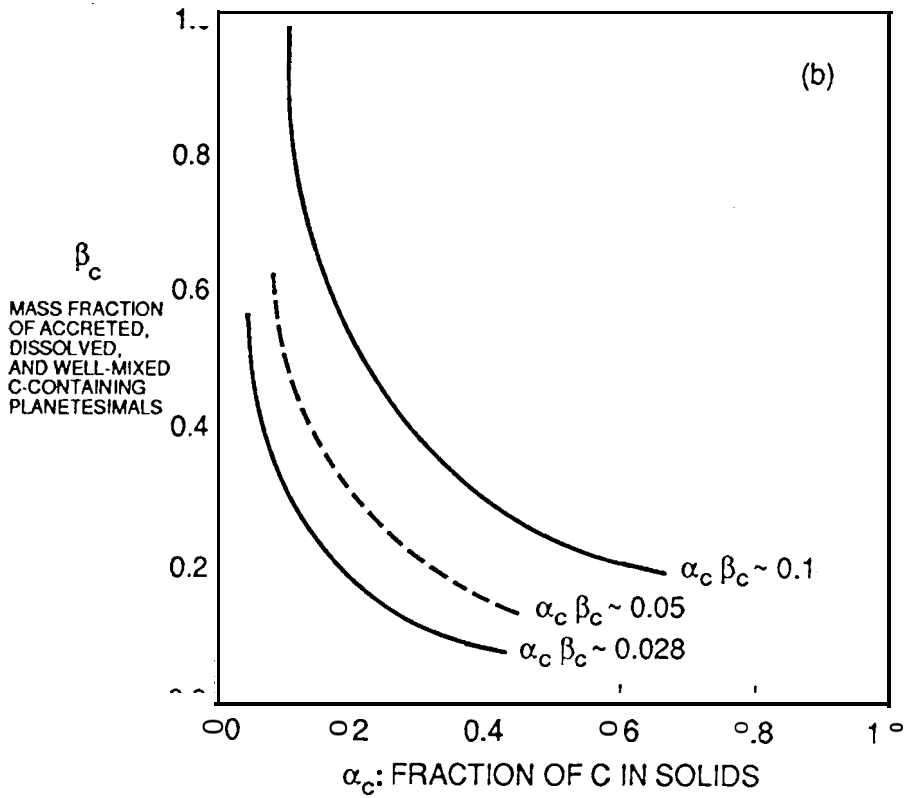
(b)
1..
0.8
0.6
0.4
0.2
β_c
MASS FRACTION OF ACCRETED, DISSOLVED, AND WELL-MIXED C-CONTAINING PLANETESIMALS
$\alpha_c \beta_c$ ~ 0.1
$\alpha_c \beta_c$ ~ 0.05
$\alpha_c \beta_c$ ~ 0.028
°0
°2
0.4
°6
°.8
1 °
α_c: FRACTION OF C IN SOLIDS

FIGURE 1

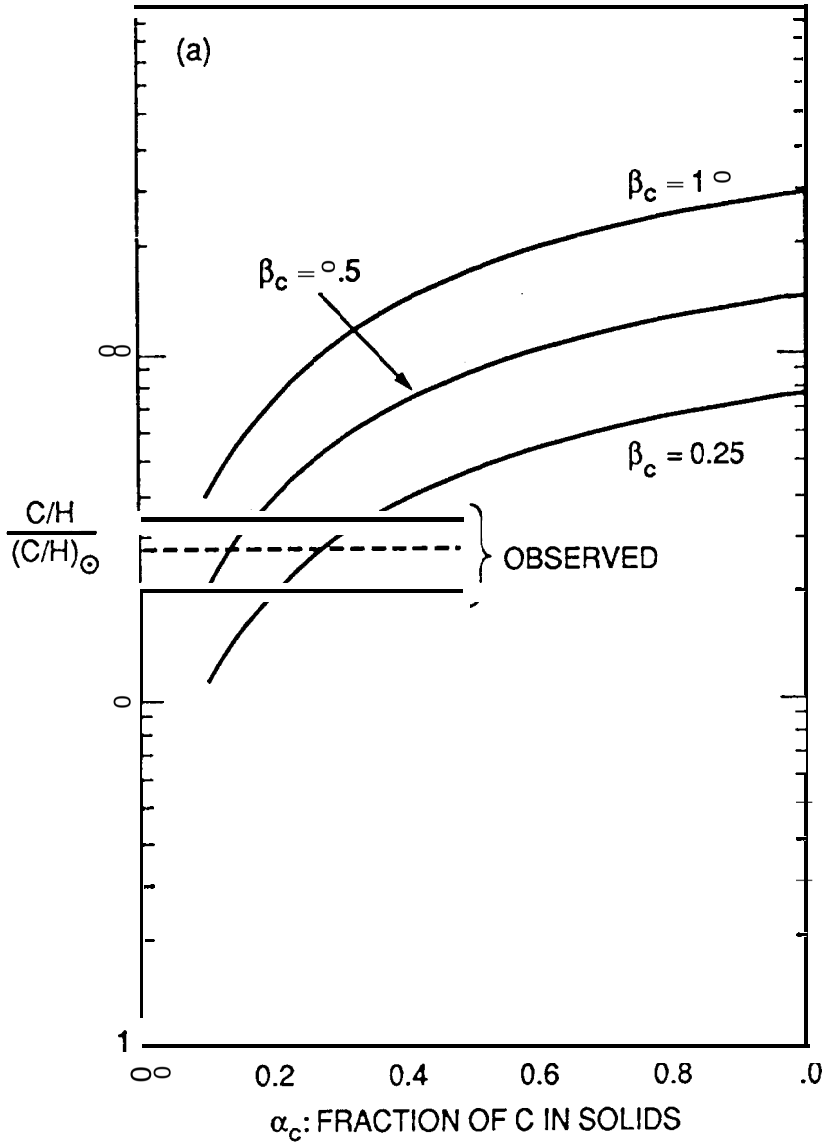
(a)
$\beta_c = 1$
$\beta_c = .5$
$\beta_c = 0.25$
C/H
$(C/H)_\odot$
OBSERVED
8
0
1
0.0
0.2
0.4
0.6
0.8
1.0
α_c: FRACTION OF C IN SOLIDS

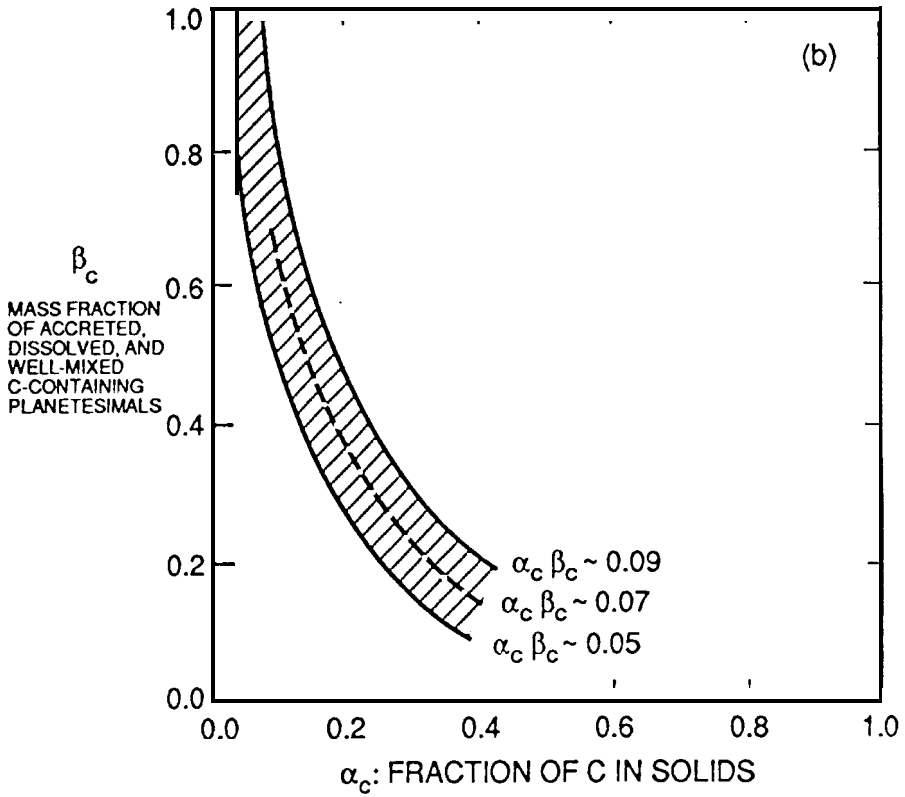
(b)
β_c
MASS FRACTION OF ACCRETED, DISSOLVED, AND WELL-MIXED C-CONTAINING PLANETESIMALS
1.0
0.8
0.6
0.4
0.2
0.0
$\alpha_c \beta_c \sim 0.09$
$\alpha_c \beta_c \sim 0.07$
$\alpha_c \beta_c \sim 0.05$
0.0
0.2
0.4
0.6
0.8
1.0
α_c: FRACTION OF C IN SOLIDS

FIGURE 12

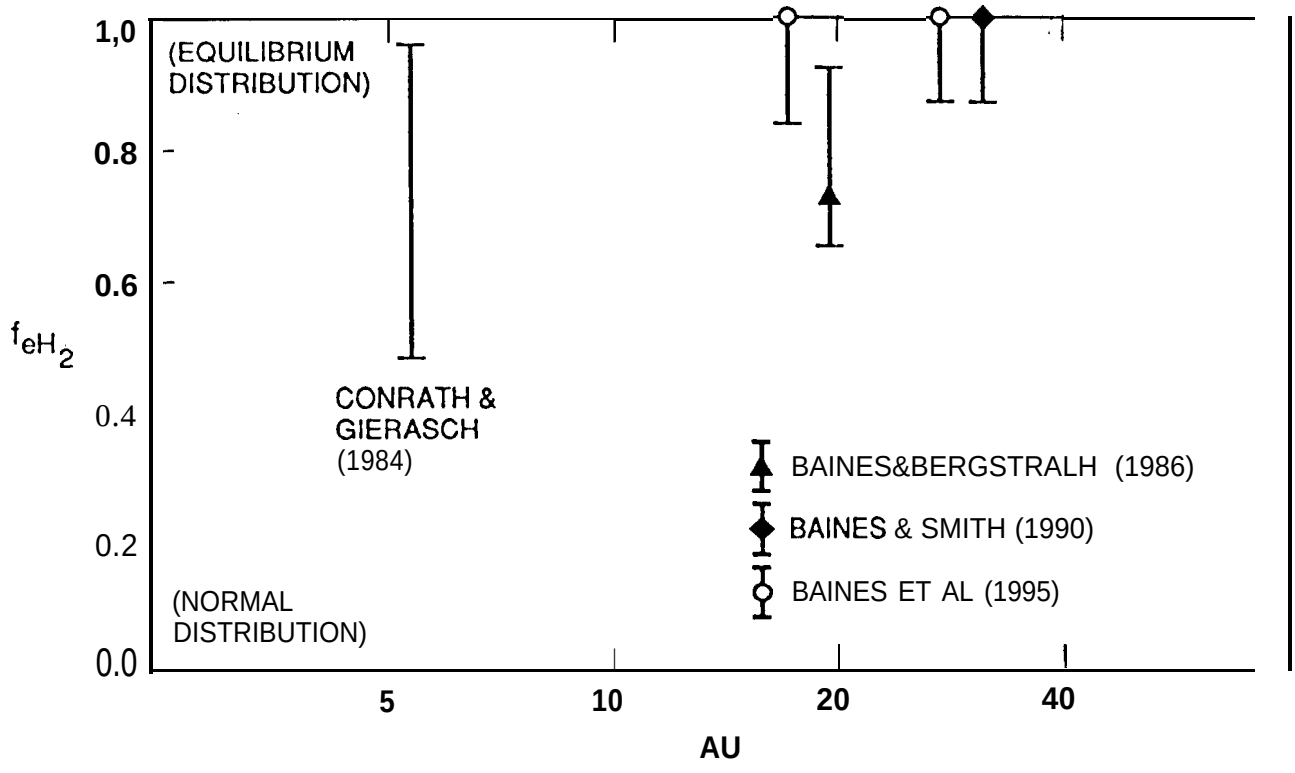
1,0
0.8
0.6
0.4
0.2
0.0
f_{eH_2}
(EQUILIBRIUM DISTRIBUTION)
(NORMAL DISTRIBUTION)
CONRATH & GIERASCH (1984)
BAINES&BERGSTRALH (1986)
BAINES & SMITH (1990)
BAINES ET AL (1995)
5
10
20
40
AU